# Supporting Information

# Polymer Nanoparticle-Based Spherical Photonic Pigments for Dye-Free Non-Iridescent Bright Coloring

*Laurinda R. P. Areias [a], Gema Marcelo [a,b], José Paulo S. Farinha [a,]**

[a] Centro de Química Estrutural and Department of Chemical Engineering, Instituto Superior Técnico, Universidade de Lisboa, 1049-001 Lisboa, Portugal

[b] Departamento de Química Analítica, Química Física e Ingeniería Química and Instituto de Investigación Química "Andrés M. Del Rio"(IQAR), 28805, Universidad de Alcalá, Alcalá de Henares, Madrid, Spain

*farinha@tecnico.ulisboa.pt

## Contents

## 1. Characterization of polymer nanoparticles (PNP) and polydopamine (PD) nanoparticles

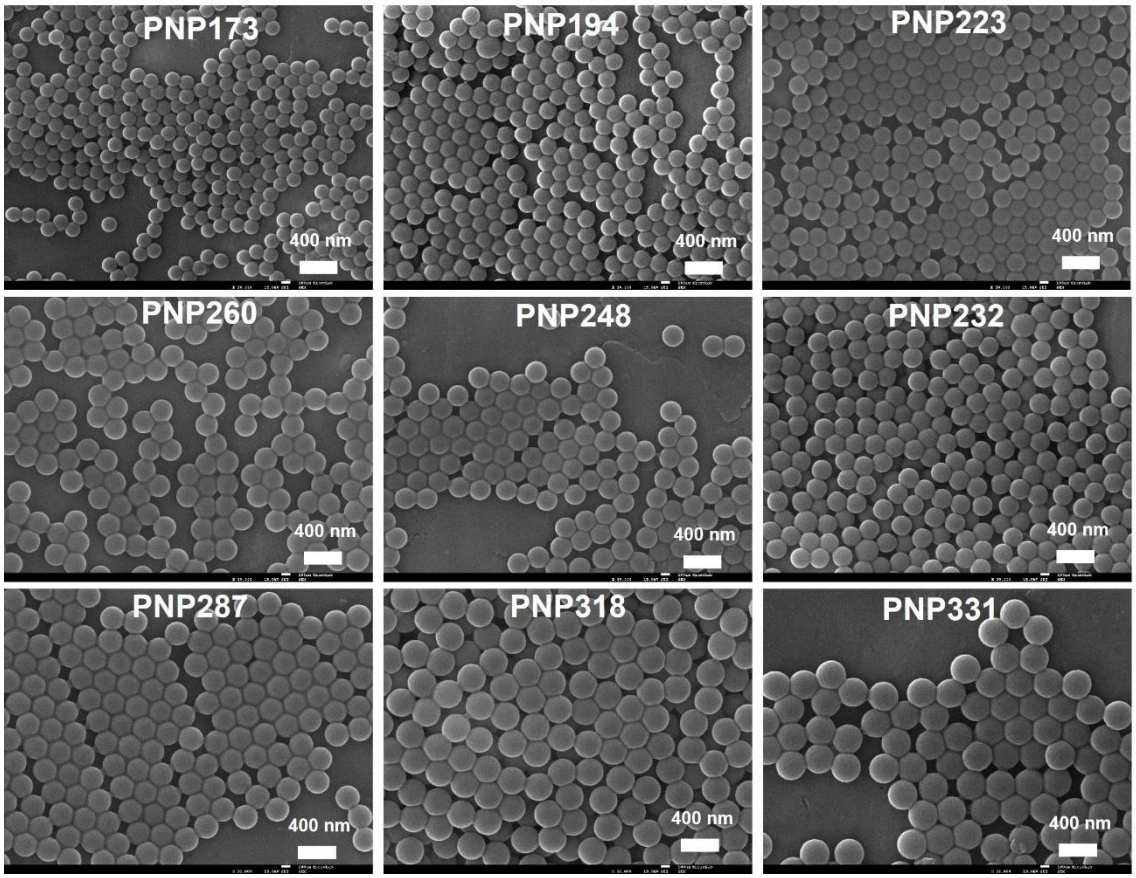


**Figure S1.** SEM images of polymer nanoparticles (PNP) of different diameters (173 nm to 331 nm), obtained by using decreasing amounts of surfactant (SDS) in the polymerization.

**Table S1.** Polymer nanoparticles (PNP) diameter measured by DLS and SEM.

| Sample | PNP Code | [SDS]/M | PNP diameter (nm) | | PDI[b] (%) |
|---|---|---|---|---|---|
| | | | DLS[a] | SEM | |
| 1 | PNP173 | $1.39x10^{-3}$ | 172 | 173 | 2.5 |
| 2 | PNP194 | $1.16x10^{-3}$ | 203 | 194 | 3.2 |
| 3 | PNP223 | $1.01x10^{-3}$ | 220 | 223 | 1.9 |
| 4 | PNP232 | $8.67x10^{-4}$ | 241 | 232 | 2.0 |
| 5 | PNP248 | $7.22x10^{-4}$ | 245 | 248 | 2.8 |
| 6 | PNP260 | $6.10x10^{-4}$ | 270 | 260 | 2.5 |
| 7 | PNP287 | $4.45x10^{-4}$ | 275 | 287 | 3.1 |
| 8 | PNP318 | $3.61x10^{-4}$ | 334 | 318 | 3.3 |
| 9 | PNP331 | $3.09x10^{-4}$ | 352 | 331 | 2.1 |

[a] Hydrodynamic diameter; [b] Size polydispersity index (PDI) from SEM measurements.

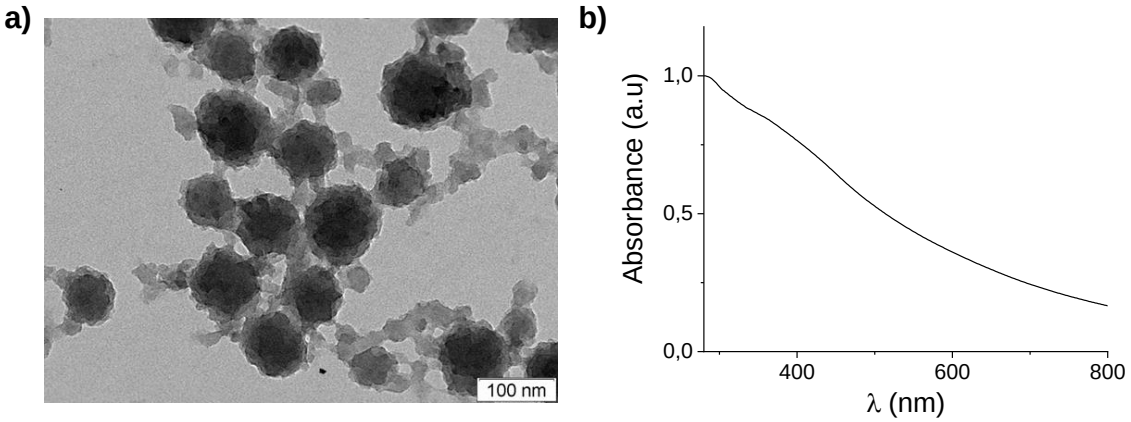


**Figure S2. a)** TEM image of polydopamine (PD) nanoparticles with 92 nm average diameter. The nanoparticles are spherical in shape but polydisperse in size. **b)** Absorption spectra of the PD nanoparticles.

## 2. Optical characterization of the photonic pigments

The angular dependence of the colors reflected by the photonic pigments was measured with a multi-angle probe holder, using white light from a tungsten light source at 45º incidence and collecting the reflectance at angles from 0º (backscattering angle) to 75º (Figure S3).

The wavelengths of maximum reflectance were predicted by Bragg-Snell's law:

$$\lambda_{max} = 2d_{hkl}n_{eff}\sqrt{1 - \frac{sin^2\theta}{n_{eff}^2}} \qquad (\mathbf{S1})$$

The interference of an incident beam within the crystal is fulfilled for $\lambda_{max}$ (that corresponds to the wavelength of the maximum reflectance); $d_{hkl}$ is the crystallographic plane; $\theta$ is the angle of incidence/collection; and $n_{eff}$ is the effective refractive index of the structure. The reflectance maximum corresponds to the stop-band between the lowest energy photonic bands along the Γ-L direction in reciprocal space, which corresponds to the [111] direction in the real space face-centered cubic (fcc) structure. Here we consider the photonic pigments to be oriented with its Γ-L direction towards the surface of the pigments, and therefore, plane $d_{111}$ is used. In the case of close-packed nanoparticles, $d_{111}$ is calculated according to

$$d_{111} = \sqrt{2/3}\,D \qquad (\mathbf{S2})$$

where $D$ corresponds to nanoparticles diameter. The effective refractive index $n_{eff}$ of the photonic structure is the weighted average calculated according to

$$n_{eff} = \sqrt{f_{PNP}n_{PNP}^2 + f_{int}n_{int}^2} \qquad (\mathbf{S3})$$

where $f_{PNP}$ is the filling fraction of PNPs (the volume filled in the total volume of the supraparticle). The remaining volume corresponds to the interstitial voids, $f_{int}$. The refractive indices of the PNPs and the interstitial material correspond to $n_{PNP}$ and $n_{int}$, respectively. For close-packed fcc structures, the volume fractions occupied by nanoparticles is generally 0.74. The refractive index of the PNPs was calculated by averaging the dielectric constants ($\kappa = n^2$) of polystyrene ($n_{PS}$=1.592), poly(methyl methacrylate) ($n_{PMMA}$== 1.473) and poly(acrylic acid) ($n_{PAA}$=1.527) according to their molar fraction in the PNPs: $n_{PNP} = \sqrt{0.87 \times n_{PS}^2 + 0.05 \times n_{PMMA}^2 + 0.08 \times n_{PAA}^2}$.

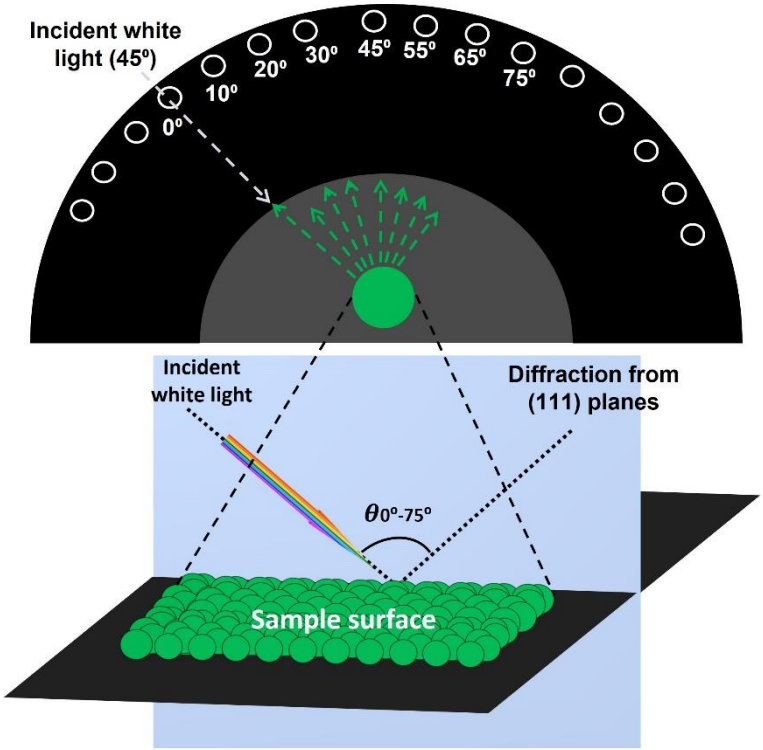


**Figure S3.** Schematic representation of the experimental set-up for angle-resolved reflectance measurements. Photonic samples are placed in a multi-angle probe holder and the sample surface is illuminated at 45º. The reflectance spectra is collected for viewing angles from 0º to 75º. Green arrows length indicates the intensity reflected for the different viewing angles. The most intense reflectance bands are obtained at the backscattering angle.

## 3. Reflectance properties of doped and undoped photonic pigments

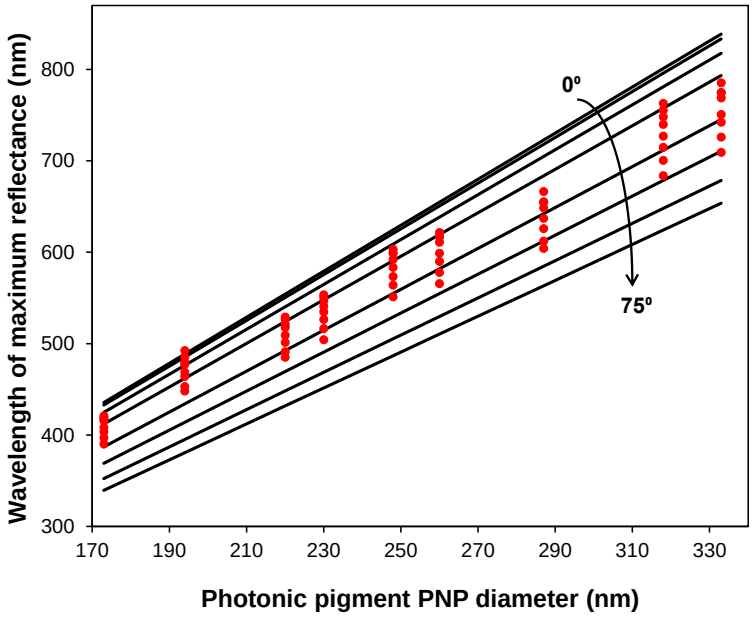


**Figure S4**. Experimental (red dots) and predicted (black lines) wavelengths of maximum reflectance for increasing collecting angles, from 0° to 75° (0°, 10°; 20°; 30°; 45°; 55°; 65° and 75° denoted by the black arrow). It is evident that spherical templating originates structures reflecting wavelengths with much lower angular dependence relative to flat structures.

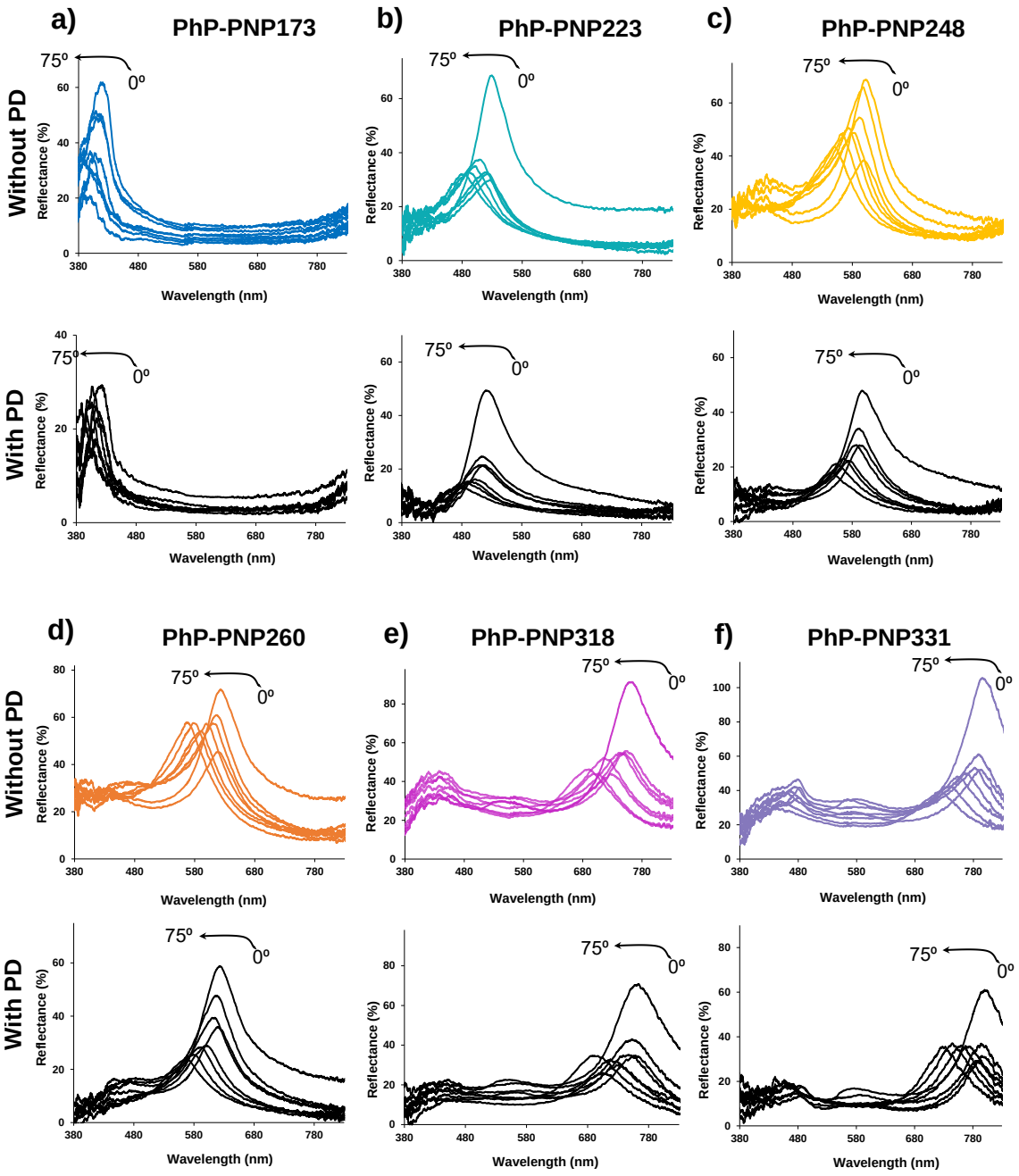


**Figure S5.** Angle resolved reflectance measurements of doped and undoped photonic pigments, at viewing angles from 0º to 75º. Deep blue PhP-PNP173 and PhP-PNP173-PD **(a)**; Cyan PhP-PNP223 and PhP-PNP223-PD **(b)**; Yellow PhP-PNP248 and PhP-PNP248-PD **(c)**; Orange PhP-PNP260 and PhP-PNP260-PD **(d)**; PhP-PNP318 and PhP-PNP318-PD **(e)** PhP-PNP331 and PhP-PNP331-PD **(f)**. Absolute intensity values cannot be compared because they depend on the amount of sample measured.

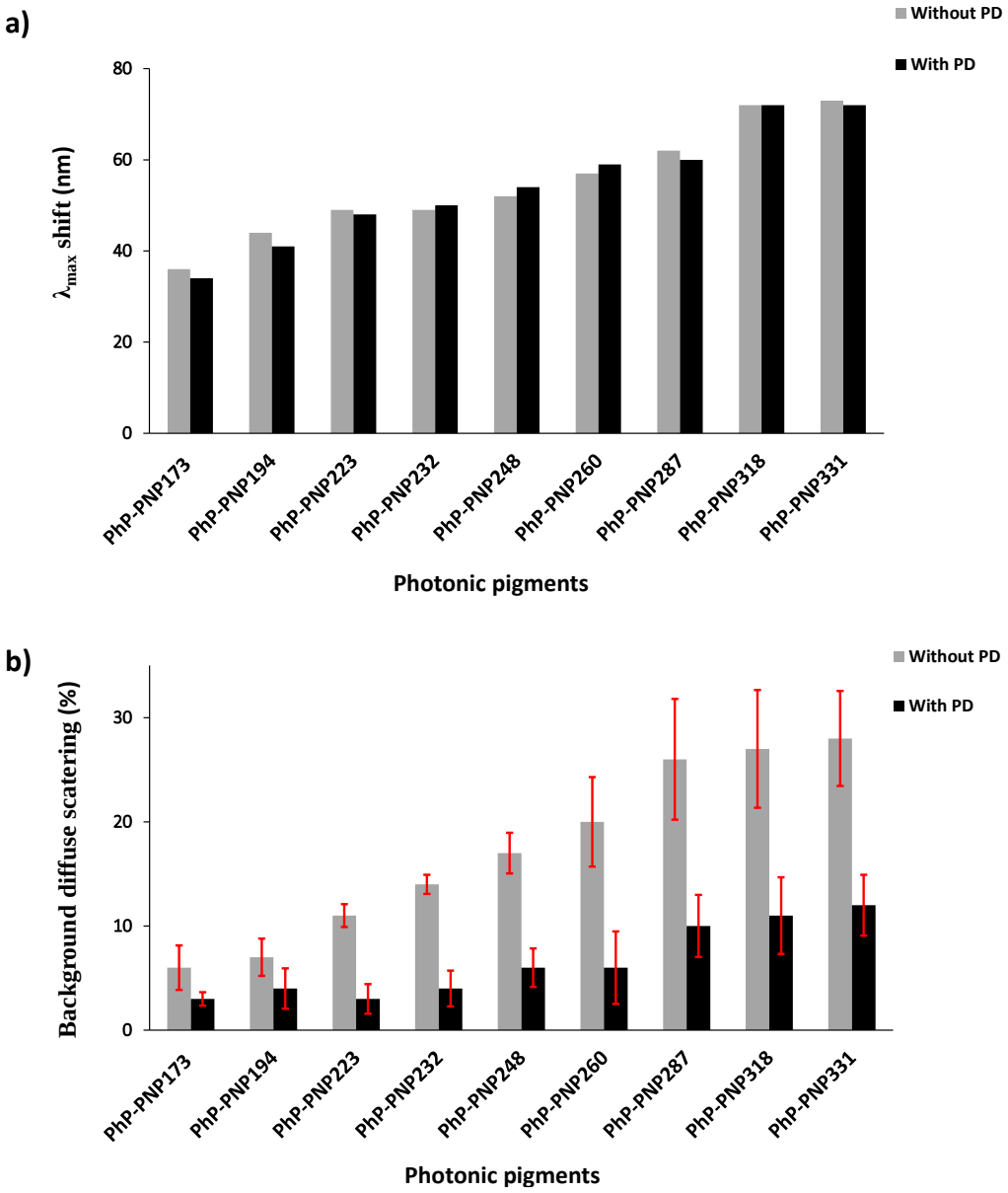


**Figure S6**: Comparison between the shift in the wavelength of maximum reflectance $\lambda_{max}$ (**a**) and the background diffuse scattering (**b**) with viewing angle (between 0° and 75°), for doped and undoped pigments. The background diffuse scattering represents the average scattering background intensity values on both sides of the reflectance bands (except for PhP-PNP173 and PhP-PNP331) for all collecting angles. The error bars correspond to the standard deviation of the background diffuse scattering of all collecting angles.

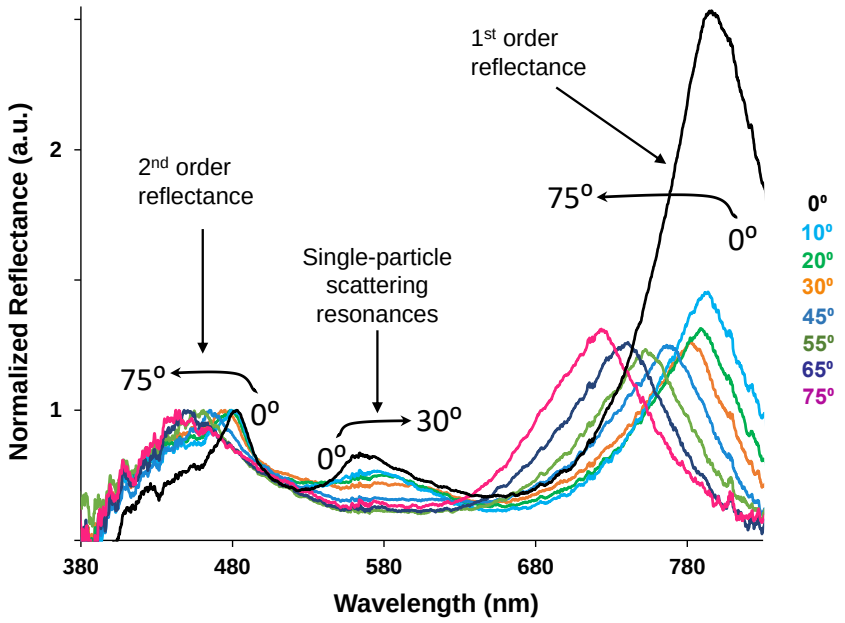


**Figure S7.** Angle resolved reflectance of PhP-PNP331, normalized to the second order reflectance band. This low intensity but sharp band appears at approximately 483 nm for the backscattering angle, and shift towards shorter wavelengths (443 nm) with increasing the collecting angle from 0° to 75°. Between the 2nd and the 1st order reflectance bands, another low intensity band associated with single-particle scattering resonances appears at 564 nm for the backscattering angle. This band slightly red shift to 579 nm with increasing the collecting angle to 30° and cease to exist for higher collecting angles.

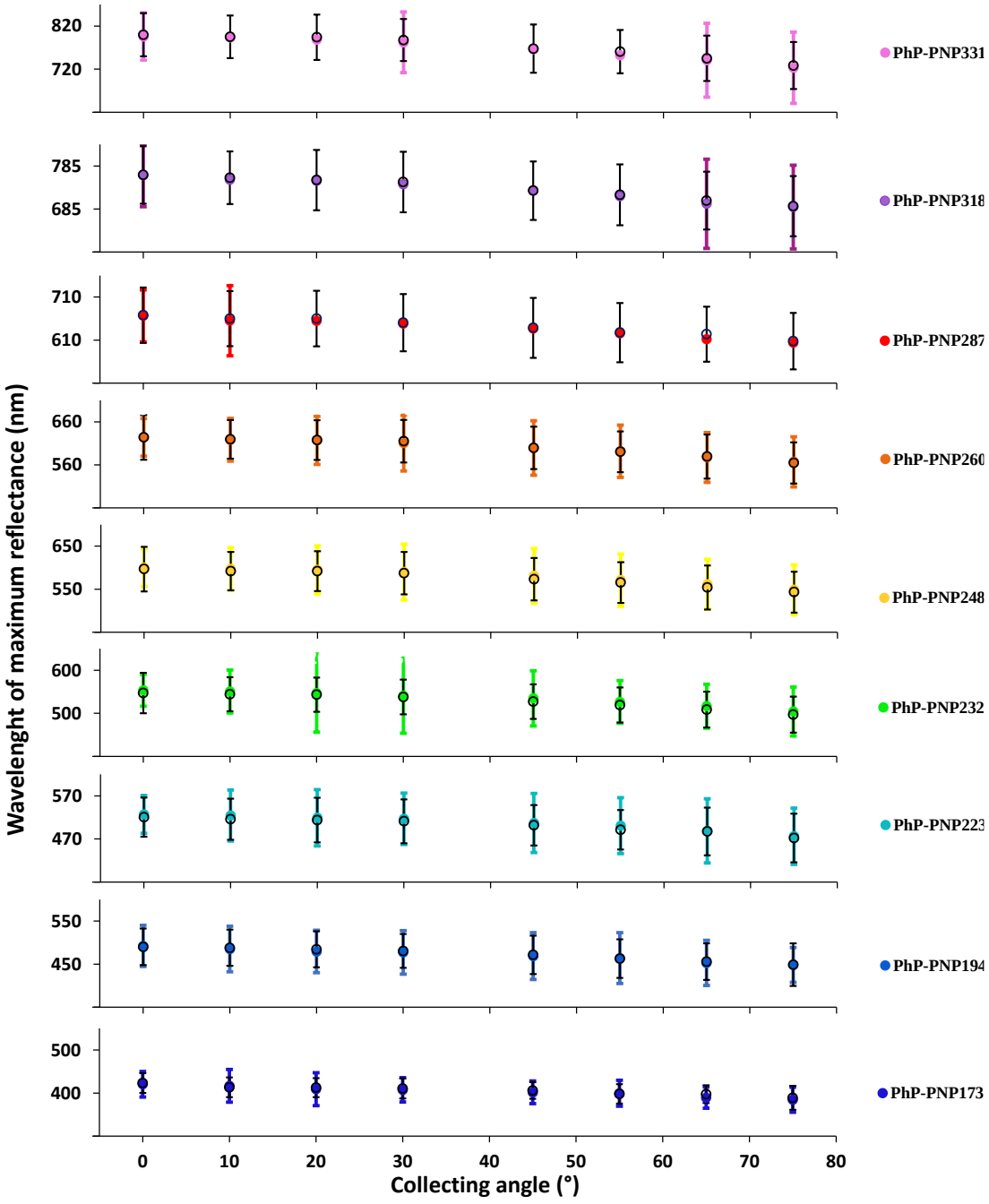


**Figure S8:** Angular dependence of the wavelength of maximum reflectance for doped (open black circles) and undoped (solid colored circles) photonic pigments, for viewing angles 0° to 75°. The bandwidth of the reflectance bands (measured as the full width at half maximum, FWHM), is represented as error bars (± FWHM/2). The colored bars correspond to the FWHM of undoped pigments (determination of the FWHM for PhP-PNP260, PhP-PNP287, PhP-PNP318 and PhP-PNP331 was not possible for all collecting angles due to the asymmetry of the reflectance bands). The black bars correspond to the FWHM of doped pigments.

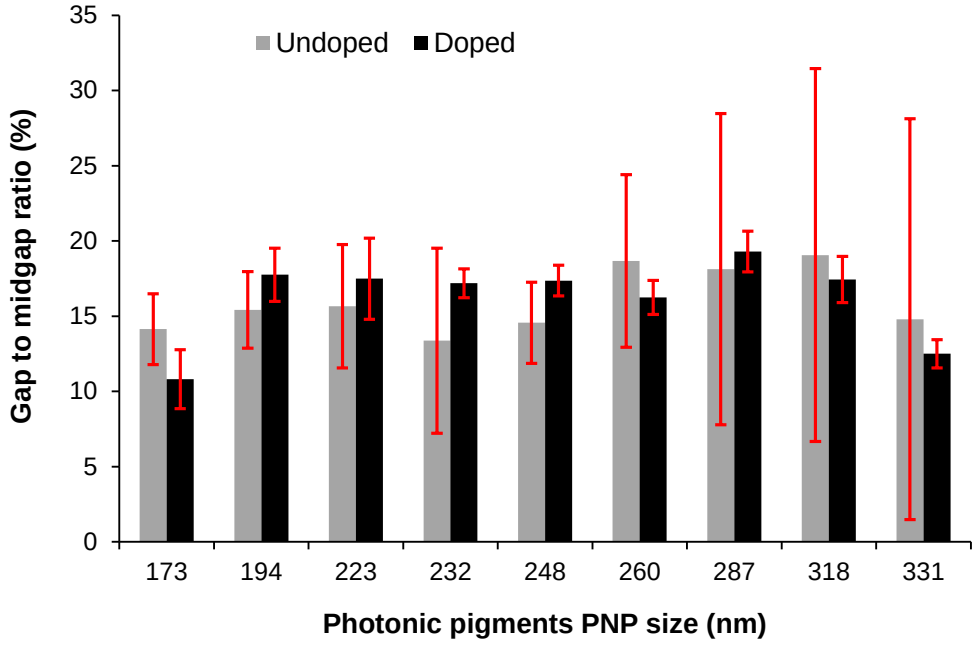


**Figure S9.** Angular dependence of the reflectance properties of doped and undoped photonic pigments. The bandwidth of the reflectance bands was used to estimate the gap to midgap ratio for doped and undoped photonic pigments. This ratio measures the relative width of the pseudo-bandgap, and corresponds to the ratio between the FWHM and the wavelength of maximum reflectance ($\Delta\lambda/\lambda_{max}$). The gap to midgap ratios, expressing the bandwidth of the stop-bands for undoped (grey bars) and doped (black bars) photonic pigments at the backscattering angle, show small differences between doped and undoped pigments. The most striking difference between the pigments is the much smaller angular dispersion (represented by the error bars, calculated as the average standard deviations of the gap to midgap ratio for collecting angles varying from 0° to 75°) of the doped pigments. This reflects the lower angular dependence of the optical properties of doped pigments.

## 4. SEM characterization of photonic pigments

**Table S2:** Diameter of the photonic pigments (PhPs) measured from SEM images for *ca.* 50 supraparticles. Formation of small satellite droplets due to possible flow fluctuations or obstruction in the microchannels can affect the size of the photonic pigments.

| Photonic pigments (PhP) | Diameter (μm) |
|---|---|
| PhP-PNP173 | 50 ± 1 |
| PhP-PNP194 | 53 ± 1 |
| PhP-PNP223 | 50 ± 1 |
| PhP-PNP232 | 55 ± 1 |
| PhP-PNP248 | 54 ± 1 |
| PhP-PNP260 | 55 ± 1 |
| PhP-PNP287 | 53 ± 1 |
| PhP-PNP318 | 54 ± 1 |
| PhP-PNP331 | 53 ± 1 |

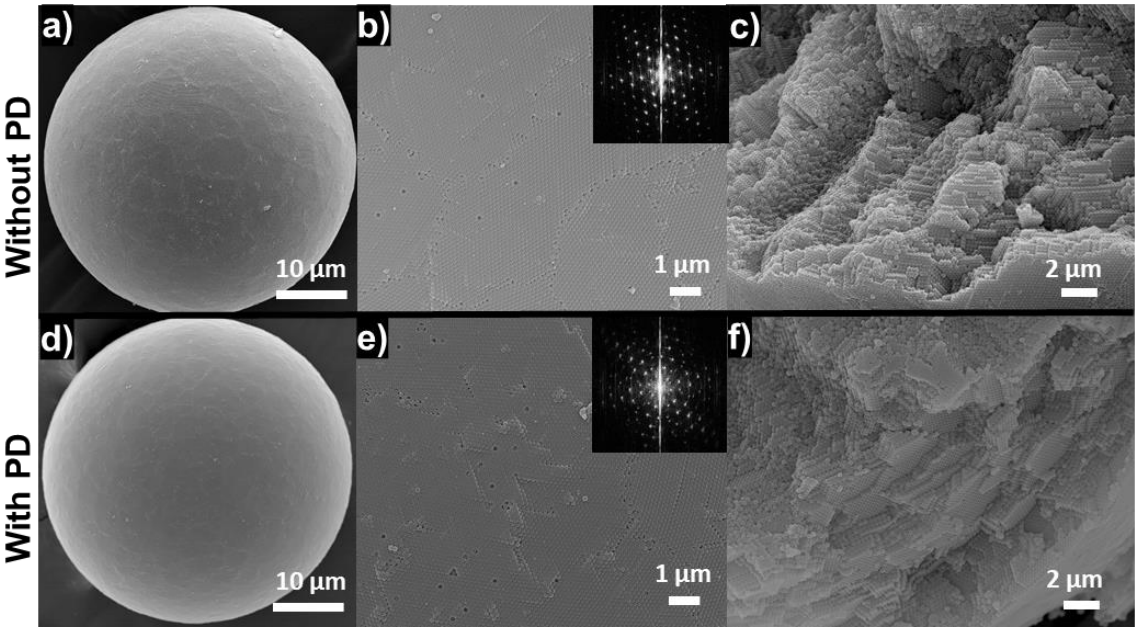


**Figure S10.** SEM images of undoped (upper panel) and doped (lower panel) photonic pigments composed of PNP173. SEM images of the spherical photonic pigments (**a** and **d**); SEM images of the pigments' surface (**b** and **e**); SEM images of the internal structure of the pigments (**c** and **f**). The 2D-FFT pattern of the surface SEM images reveals hexagonal sharp peaks confirming the presence of crystalline order. A large number of concentric ordered layers of PNP inside undoped and doped pigments is visible. The main difference between the two structures is the increased number of point defects in the surface of the pigments doped with PD. Panels **a** to **f** are enlarged in Figures S10a to S10f below.

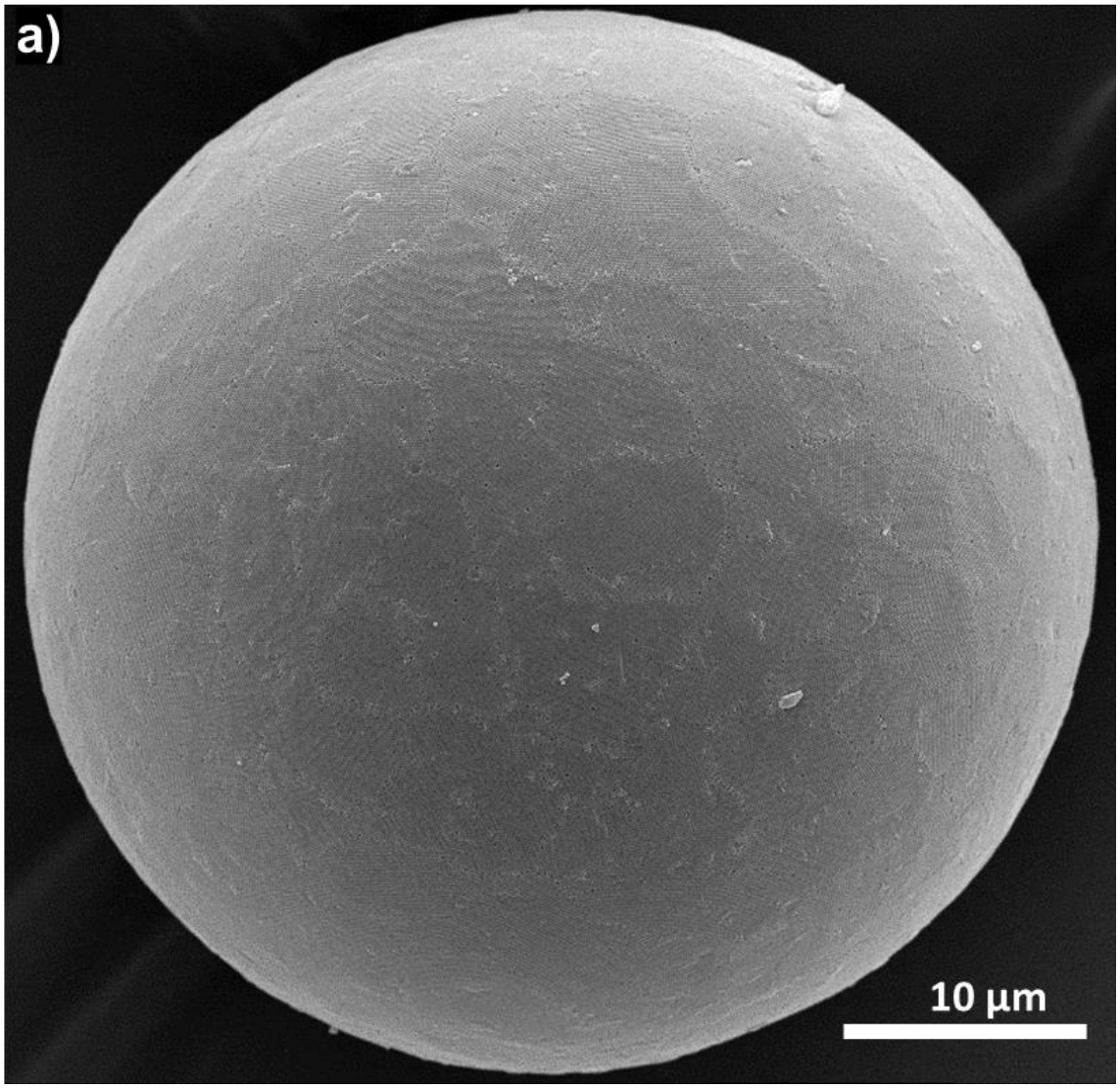


**Figure S10a:** SEM image of an undoped spherical photonic pigment assembled from PNP173.

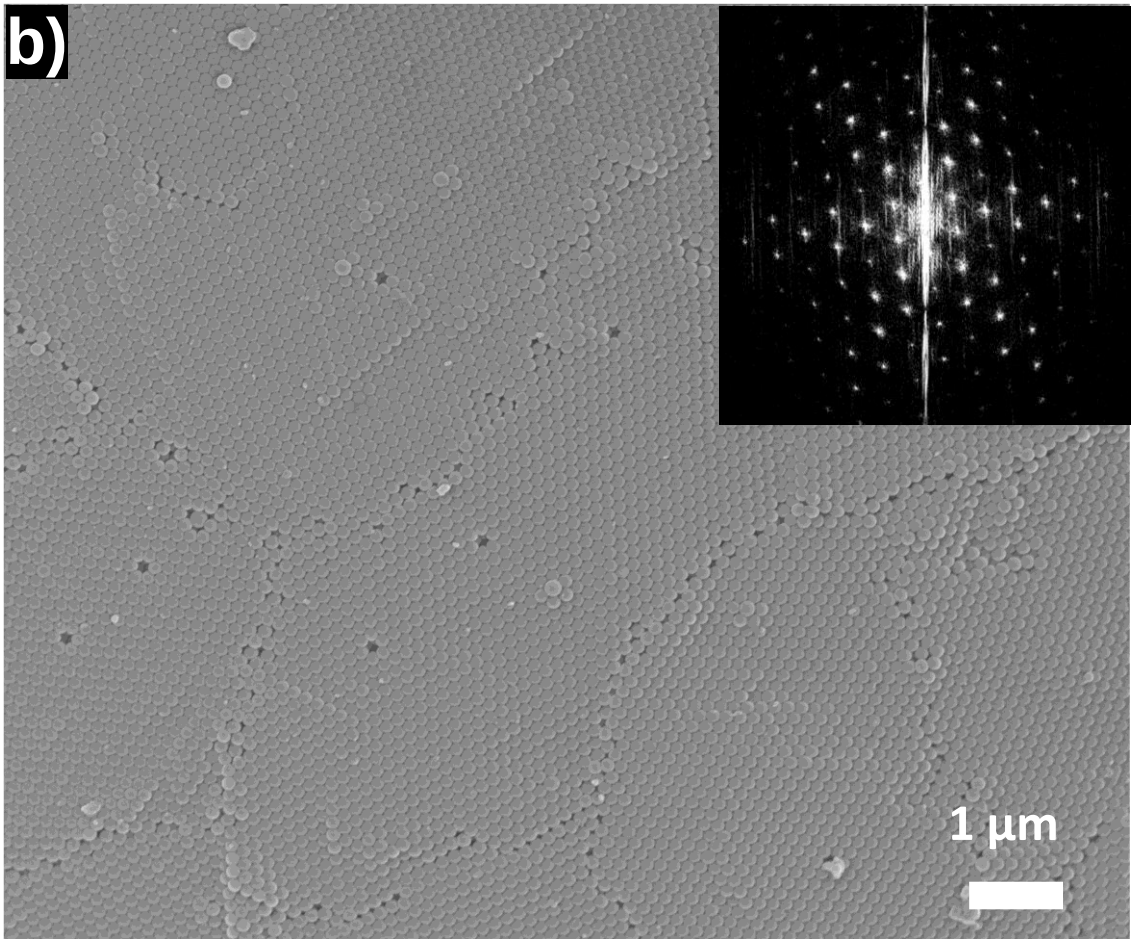


**Figure S10b:** SEM image of the surface of an undoped spherical photonic pigment assembled from PNP173.

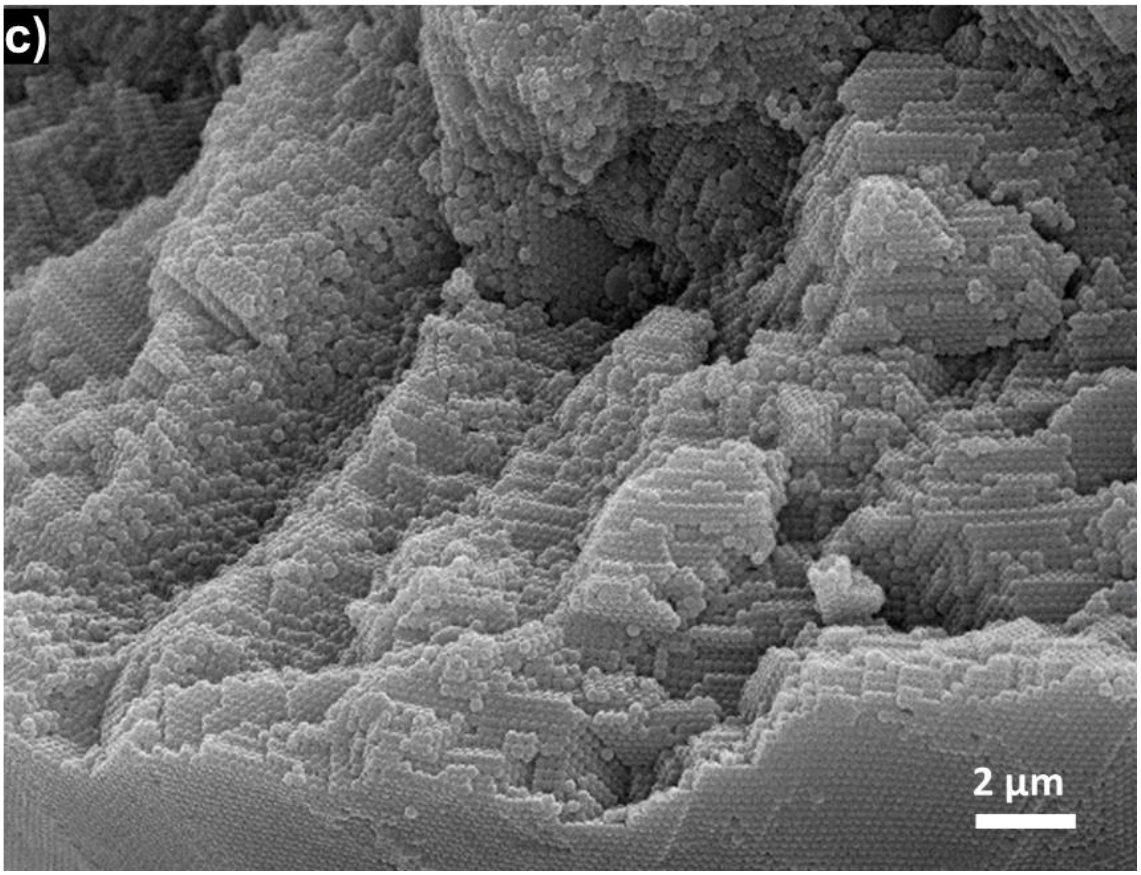


**Figure S10c:** SEM image of the internal structure of an undoped spherical photonic pigment assembled from PNP173.

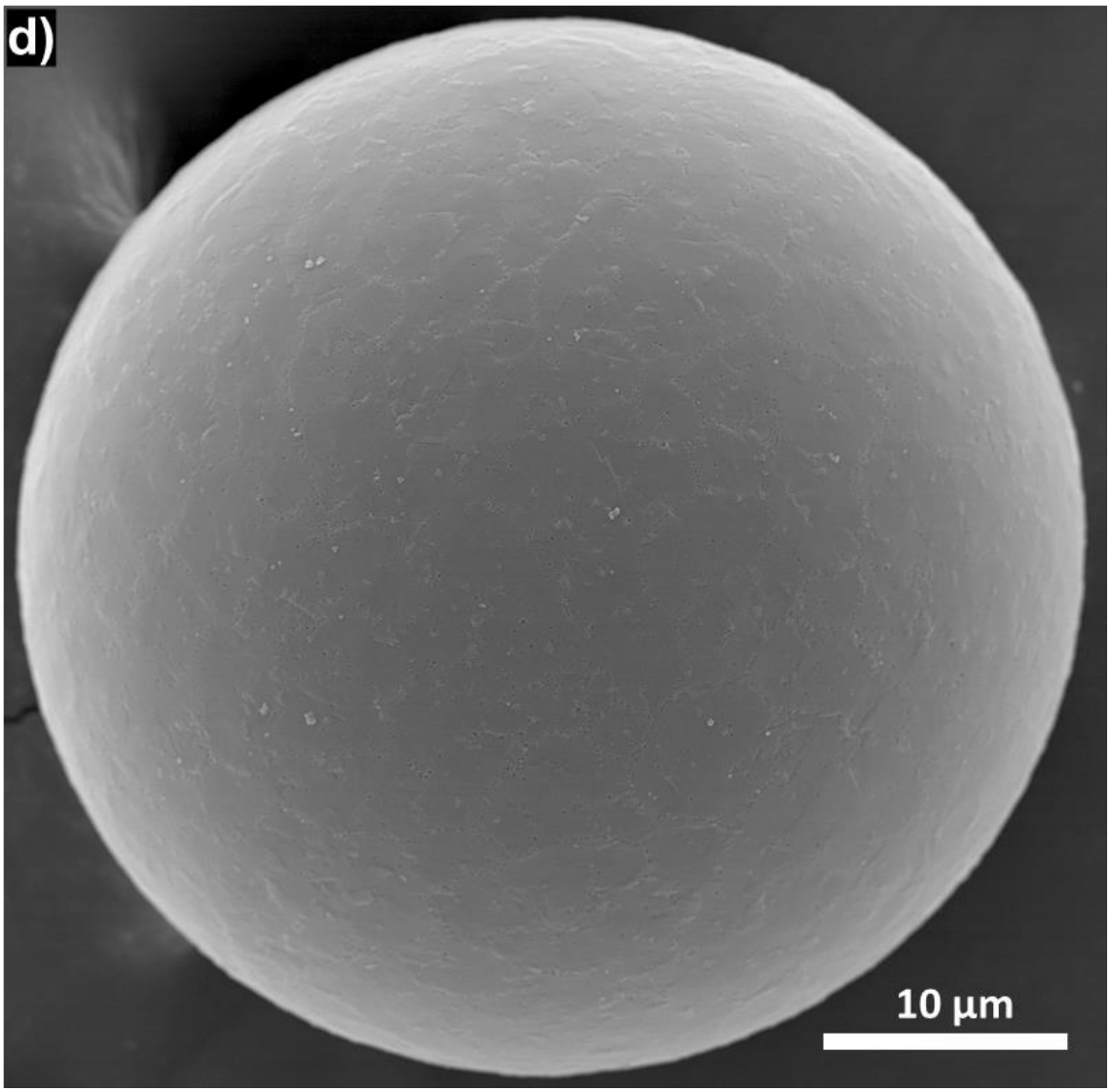


**Figure S10d:** SEM image of a doped spherical photonic pigment assembled from PNP173.

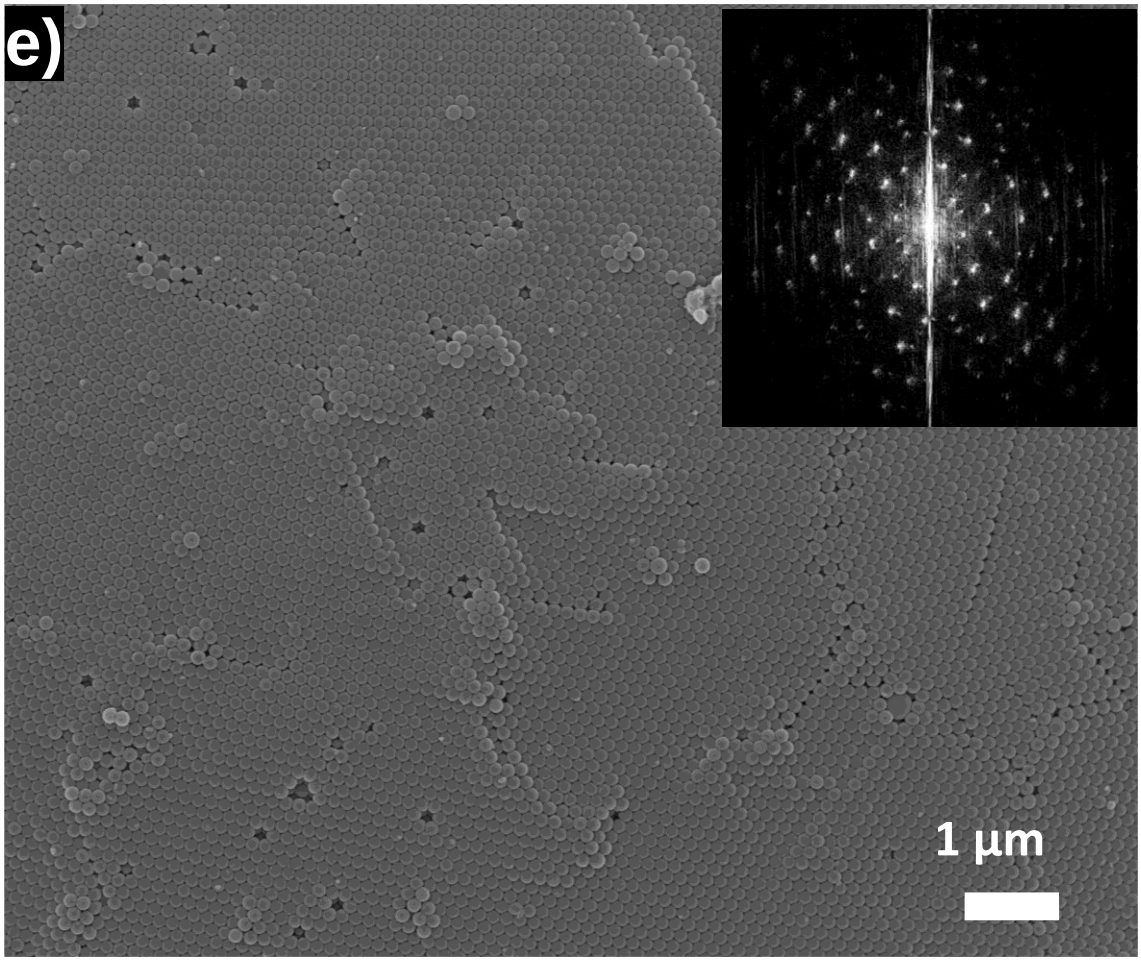


**Figure S10e:** SEM image of the surface of a doped spherical photonic pigment assembled from PNP173.

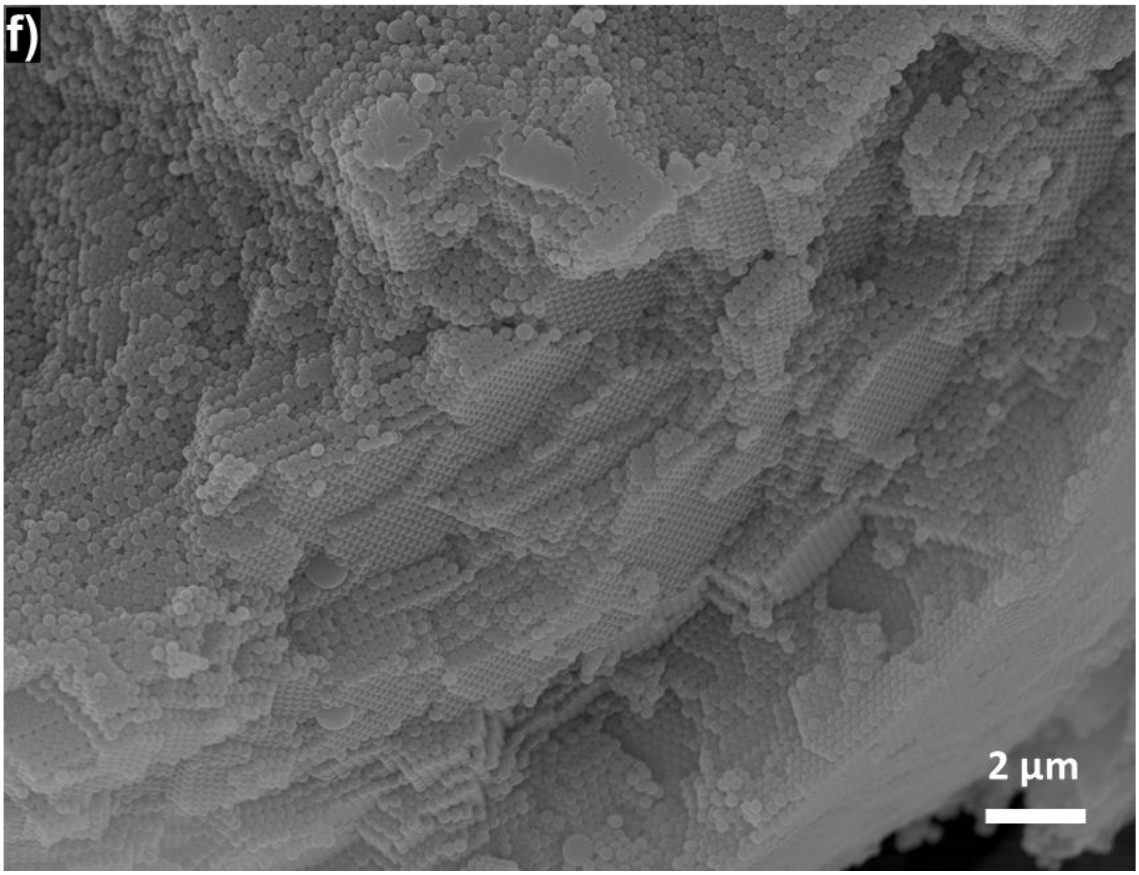


**Figure S10f:** SEM image of the internal structure of a doped spherical photonic pigment assembled from PNP173.

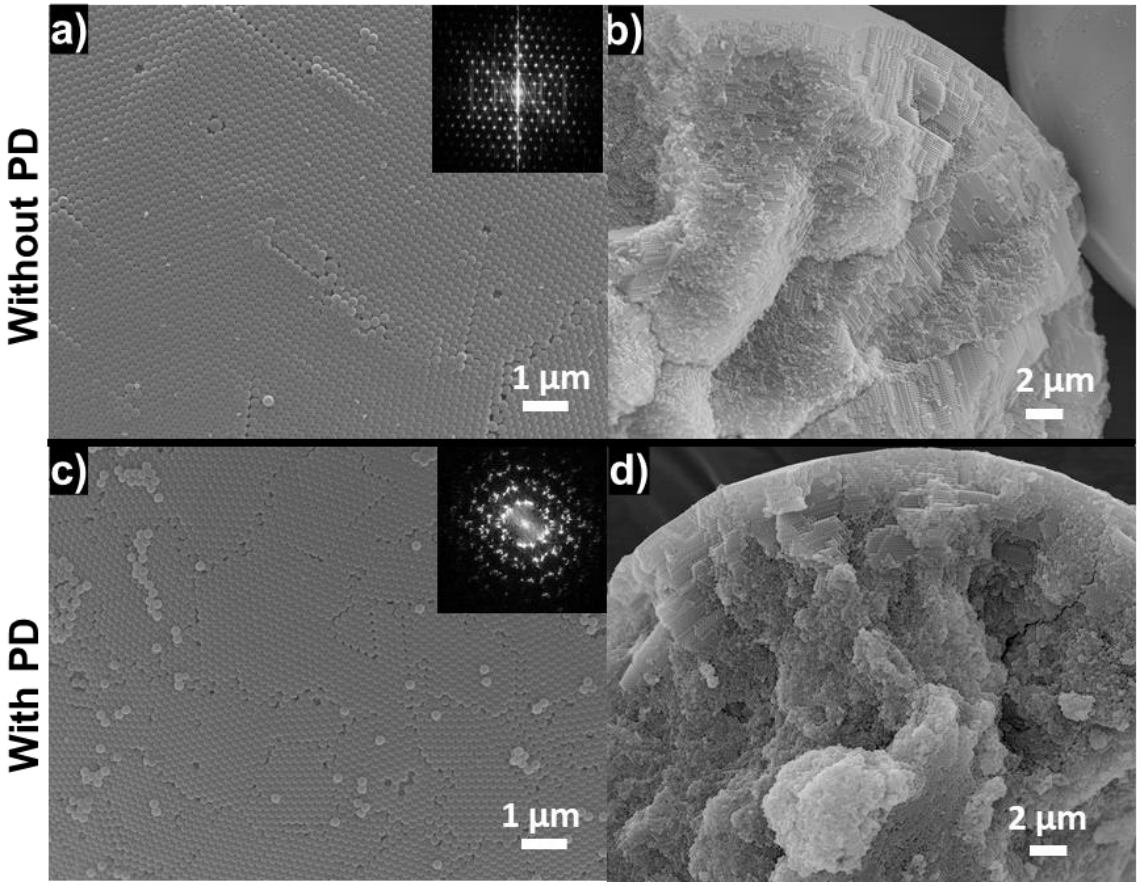


**Figure S11.** SEM images of surface (left panel) and inner structure (right panel) of undoped PhP-PNP223 (**a** and **b**) and doped PhP-PNP223-PD (**c** and **d**) pigments. Inset shows the FFT pattern from the SEM images of the pigments surface. Doped pigments present smaller crystalline domains at the surface, and a smaller number of concentric ordered PNP layers. Panels **a** to **d** are enlarged in Figures S11a to S11d below.

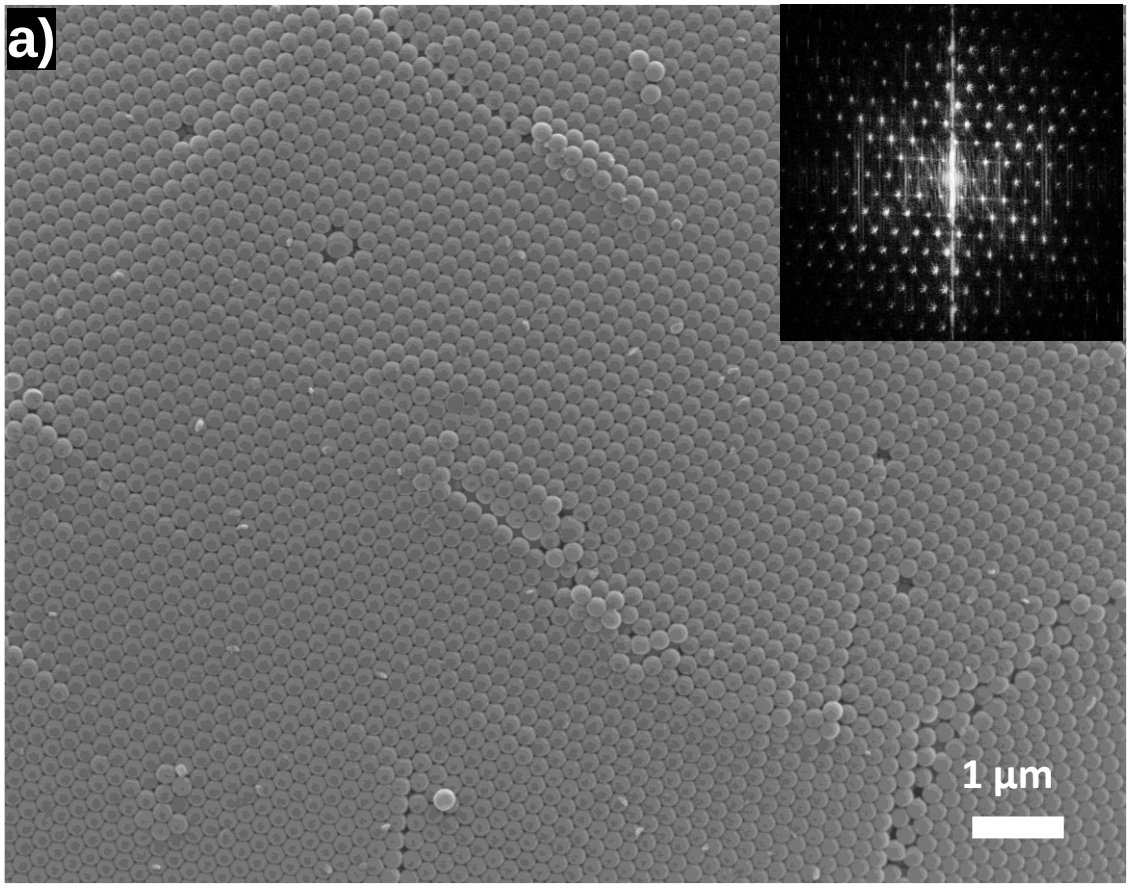


**Figure S11a:** SEM image of the surface of an undoped spherical photonic pigment assembled from PNP223.

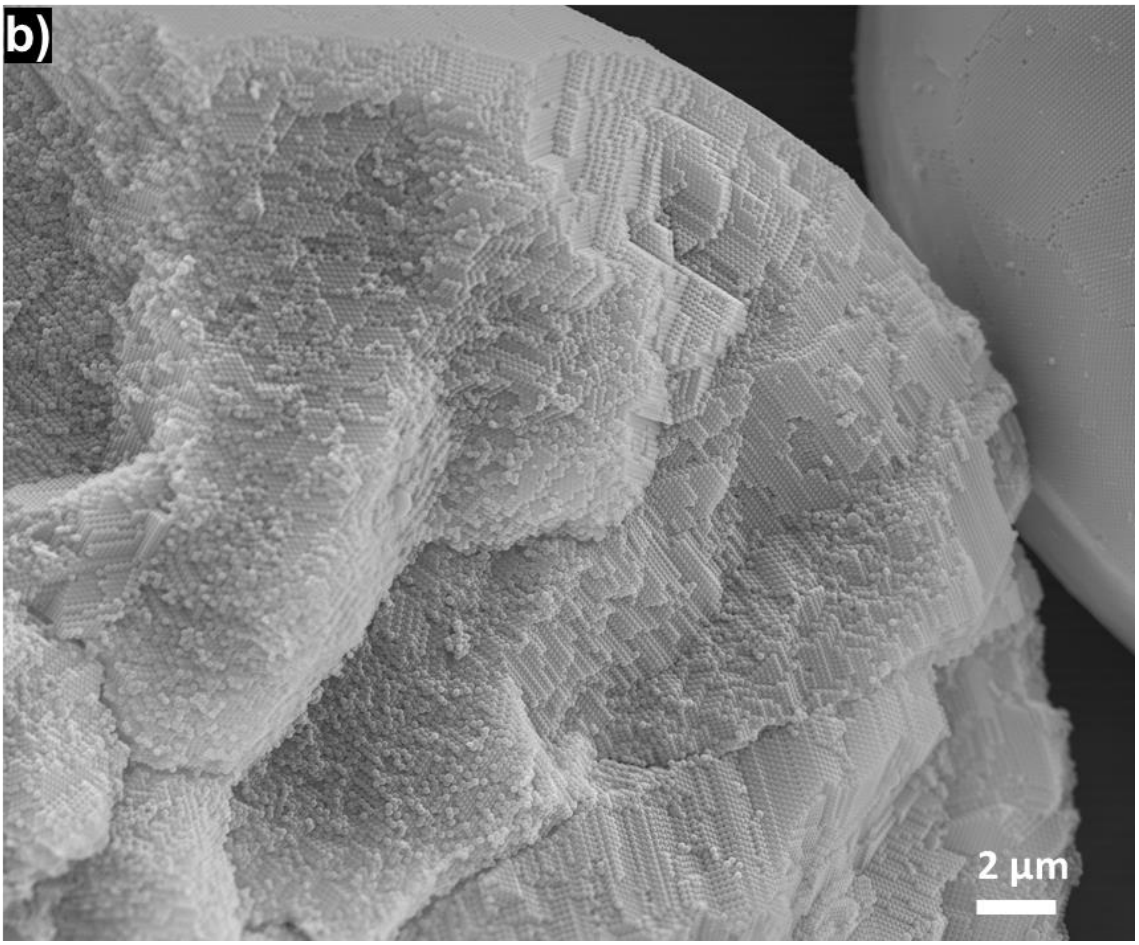


**Figure S11b:** SEM image of the internal structure of an undoped spherical photonic pigment assembled from PNP223.

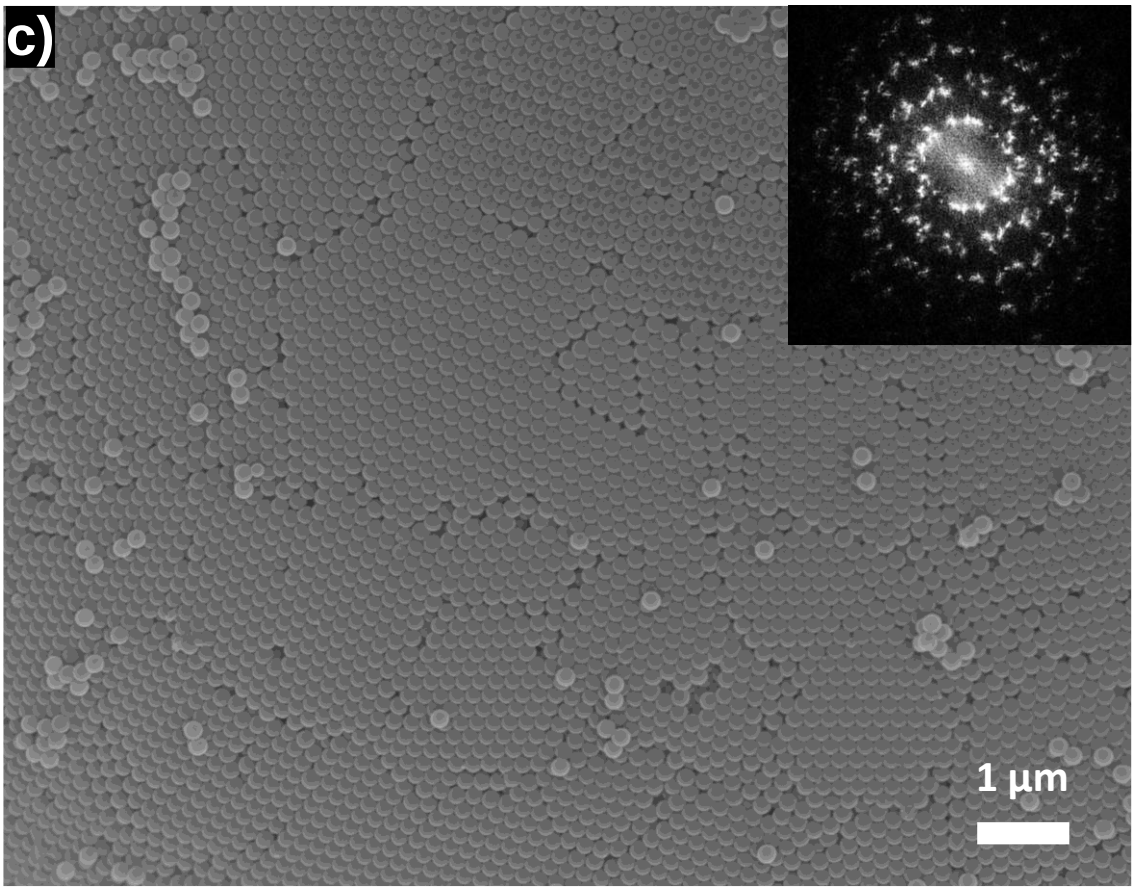


**Figure S11c:** SEM image of the surface of a doped spherical photonic pigment assembled from PNP223.

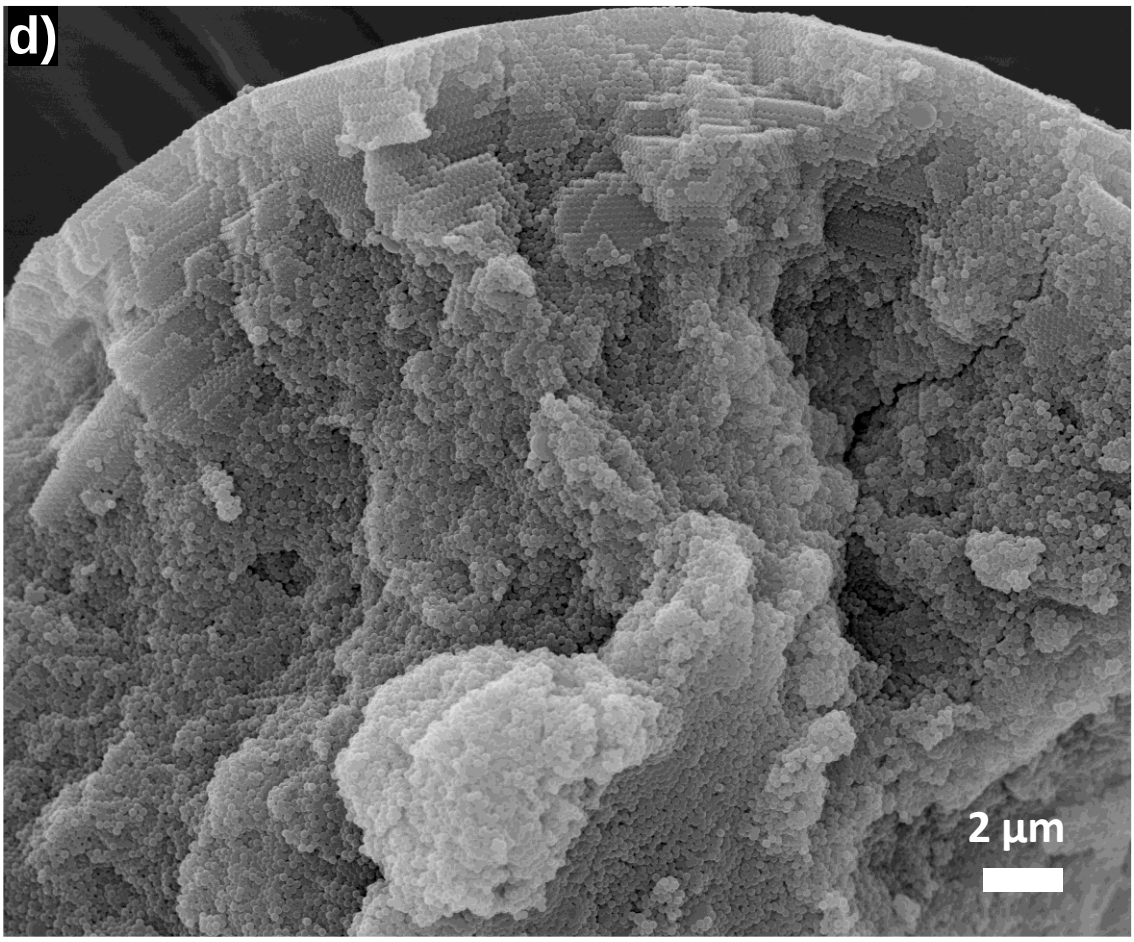


**Figure S11d:** SEM image of the internal structure of a doped spherical photonic pigment assembled from PNP223.

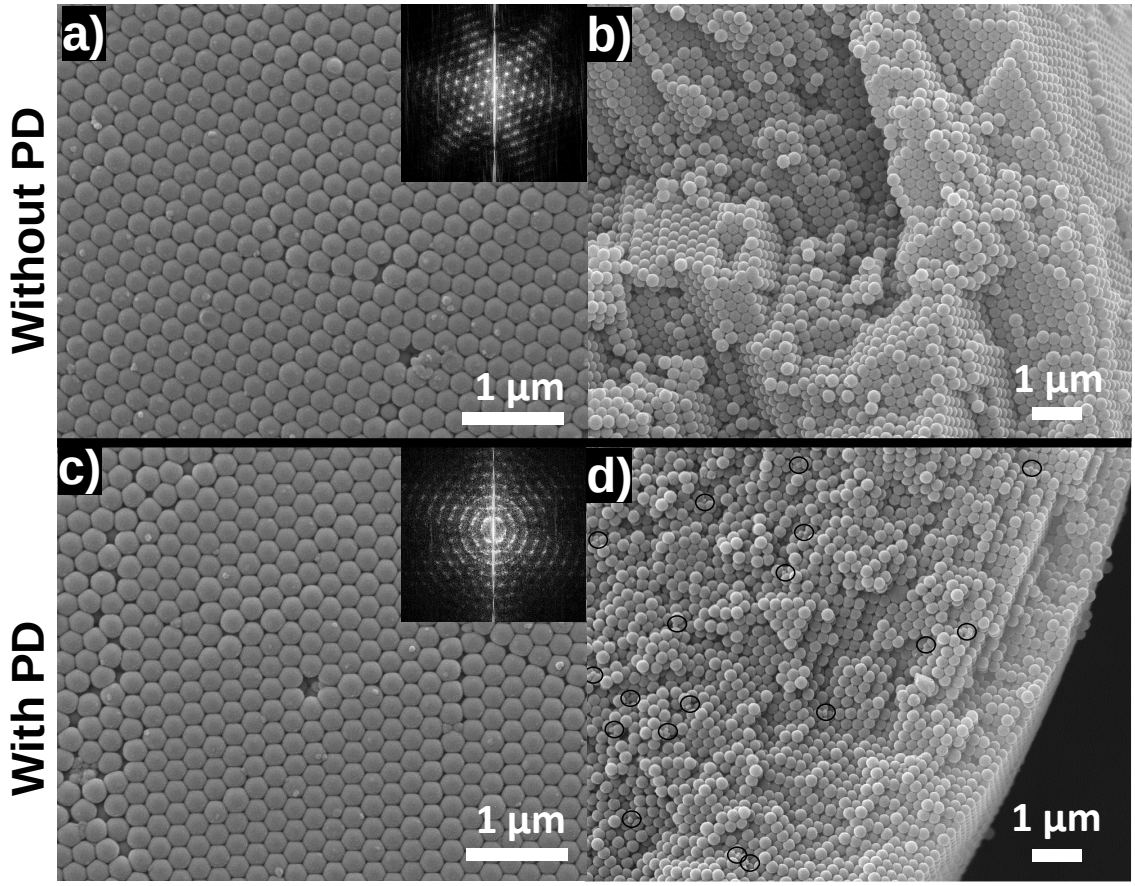


**Figure S12.** SEM images of surface (left panel) and inner structure (right panel) of undoped PhP-PNP248 (**a** and **b**) and doped PhP-PNP248-PD (**c** and **d**) pigments. Inset shows the FFT pattern from the SEM images of the pigments surface. The random distribution of PD (highlighted by the black circles in **d**) is mainly visible towards the pigments center. Undoped pigments show more ordered PNPs, both at the pigments surface and the interior. In doped pigments, only the outermost layers are orderly packed. Panels **a** to **d** are enlarged in Figures S12a to S12d below.

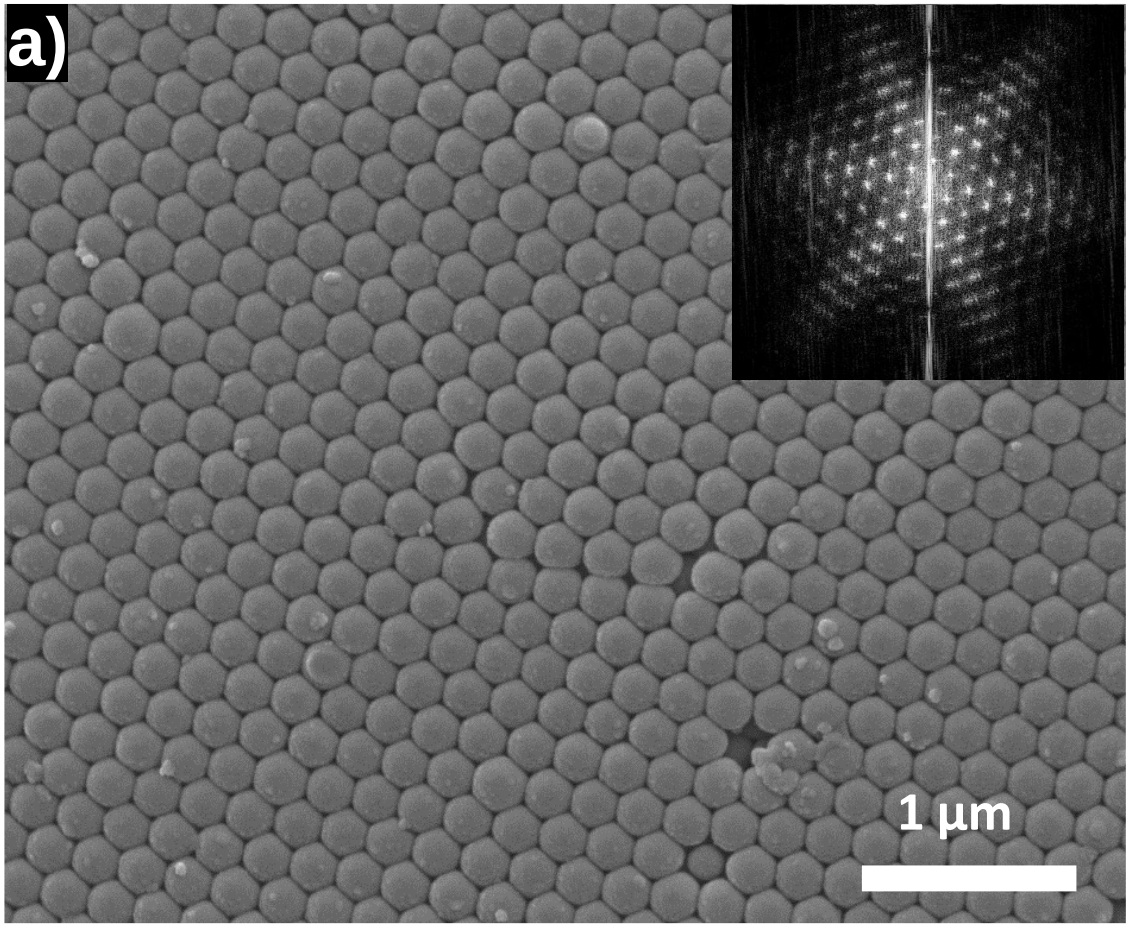


**Figure S12a:** SEM image of the surface of an undoped spherical photonic pigment assembled from PNP248.

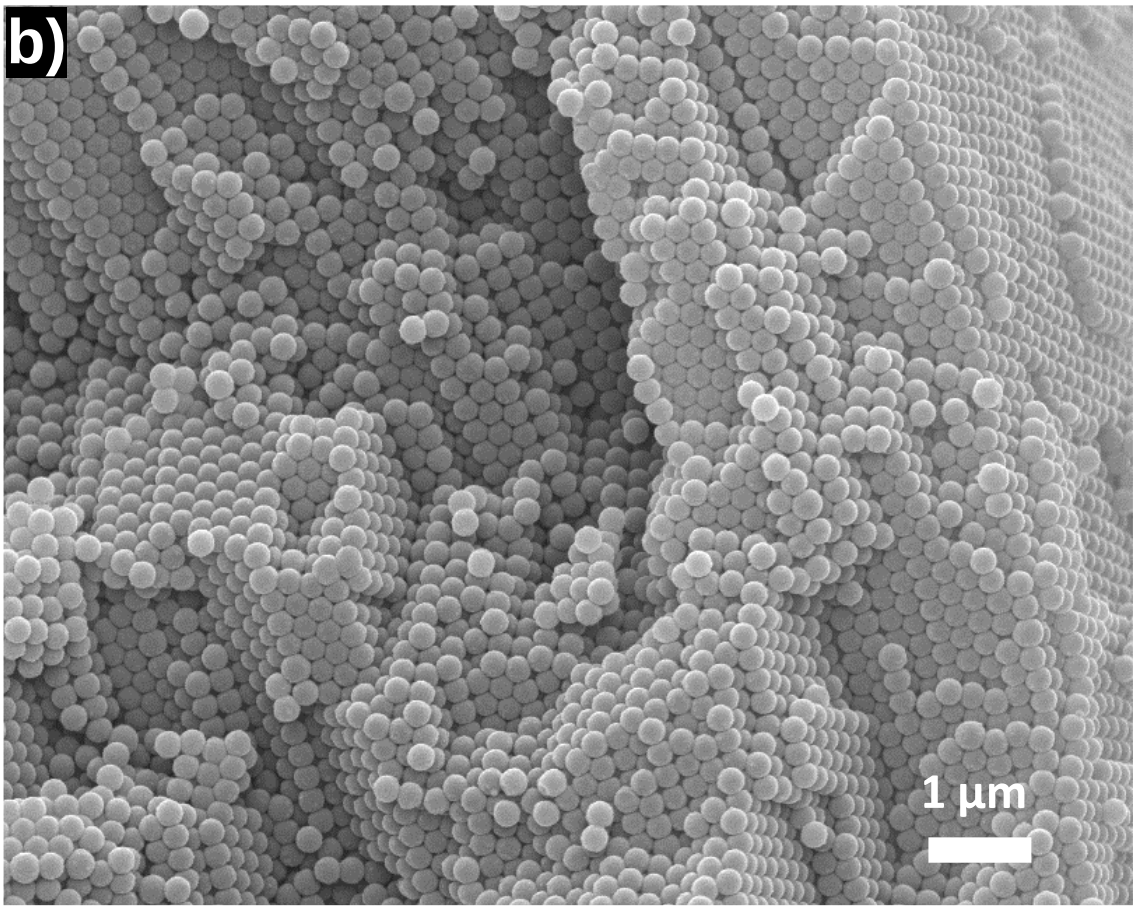


**Figure S12b:** SEM image of the internal structure of an undoped spherical photonic pigment assembled from PNP248.

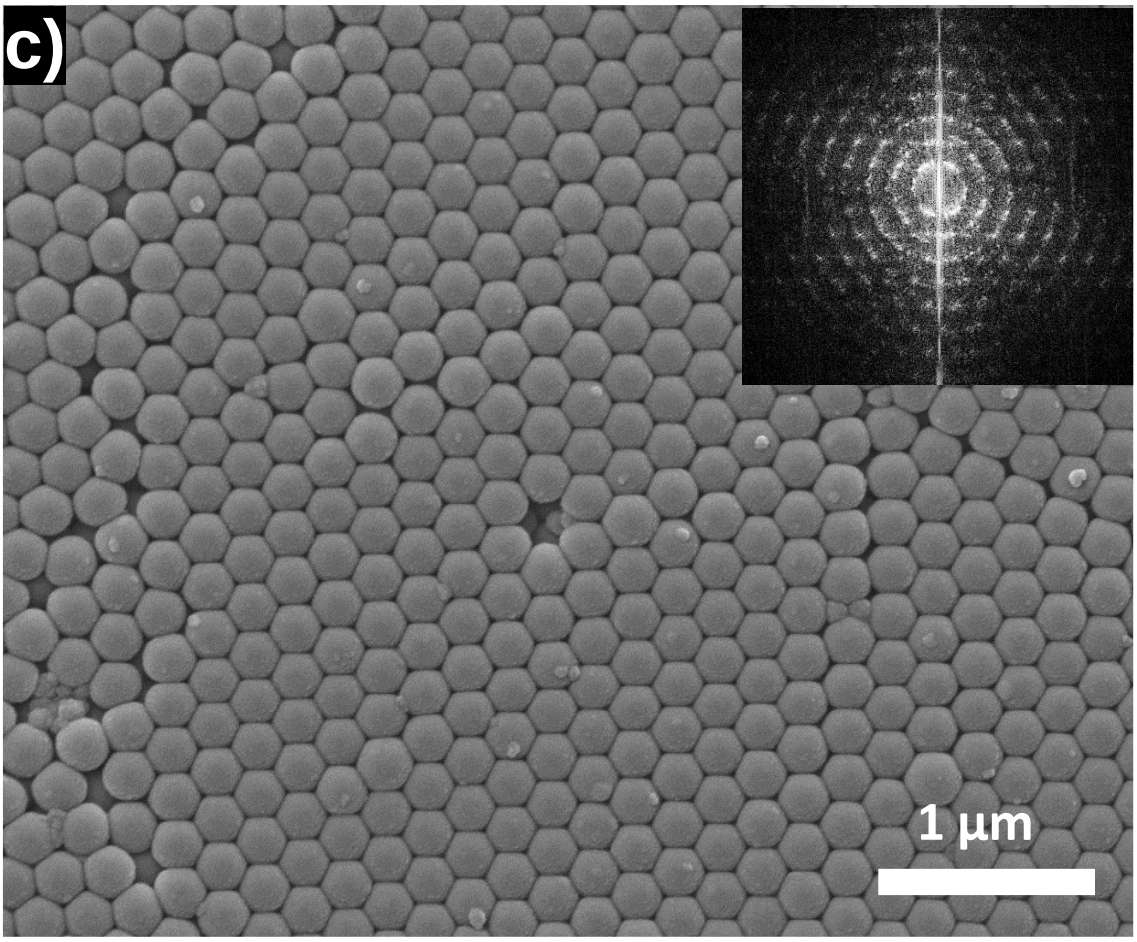


**Figure S12c:** SEM image of the surface of a doped spherical photonic pigment assembled from PNP248.

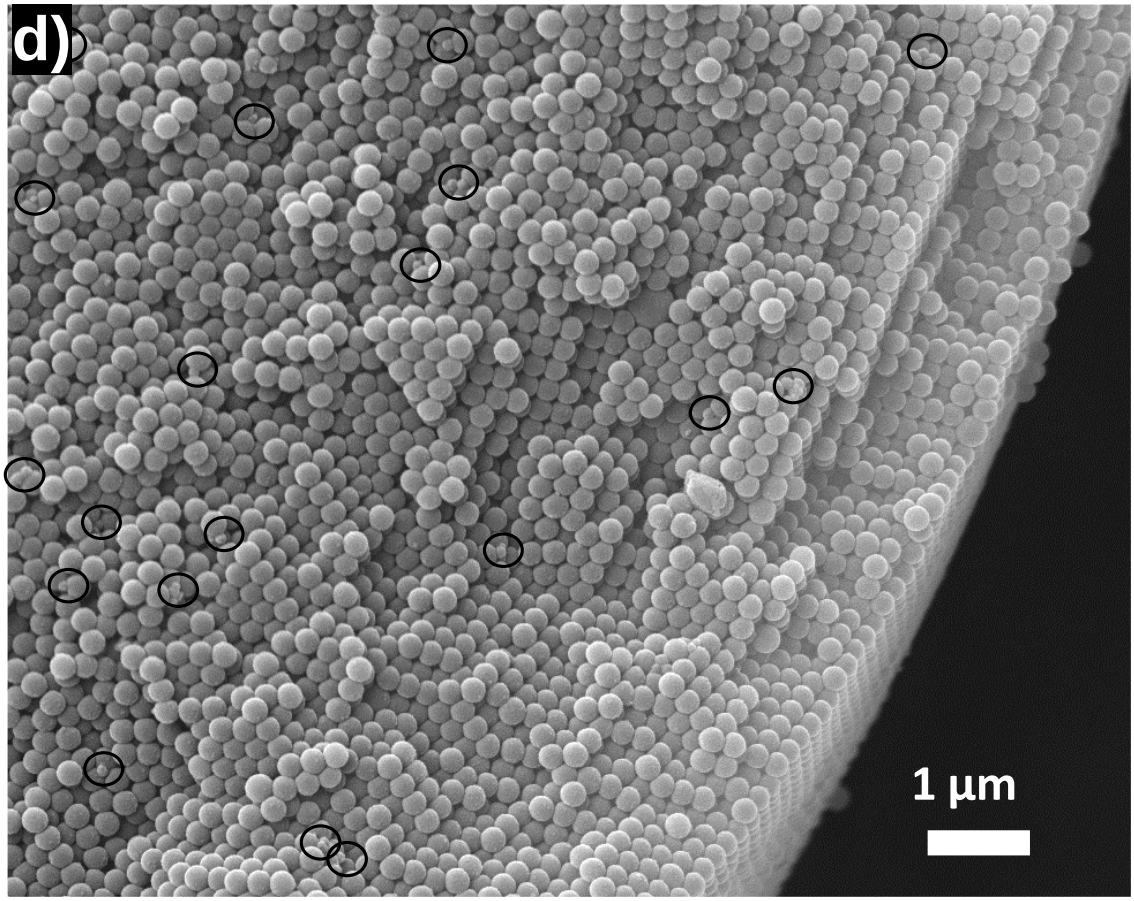


**Figure S12d:** SEM image of the internal structure of a doped spherical photonic pigment assembled from PNP248 (black circles highlight the random distribution of PD).

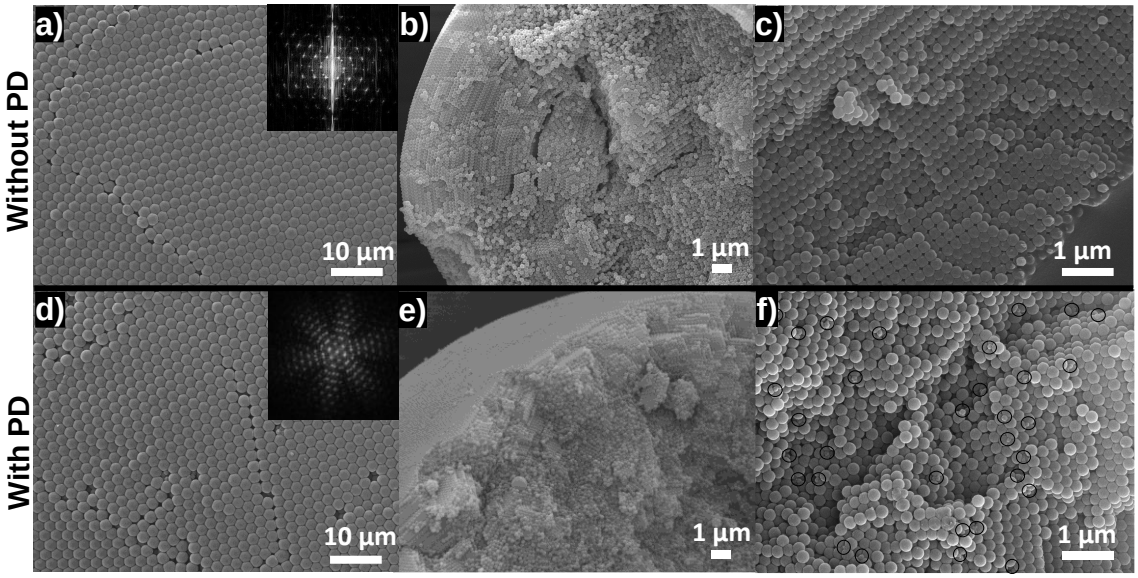


**Figure S13.** SEM images of photonic pigments composed of PNP260 undoped (upper panel) and doped with PD (lower panel). PhP-PNP260 surface (**a**) and interior (**b**); zoom in of the inner packing of PNPs (**c**). PhP-PNP260-PD surface (**d**) and interior (**e**); zoom in of the inner structure (**f**) showing the random distribution of PD (highlighted by black circles). Inset corresponds to the FFT pattern of the SEM images of the pigments surface. Panels **a** to **f** are enlarged in Figures S13a to S13f below.

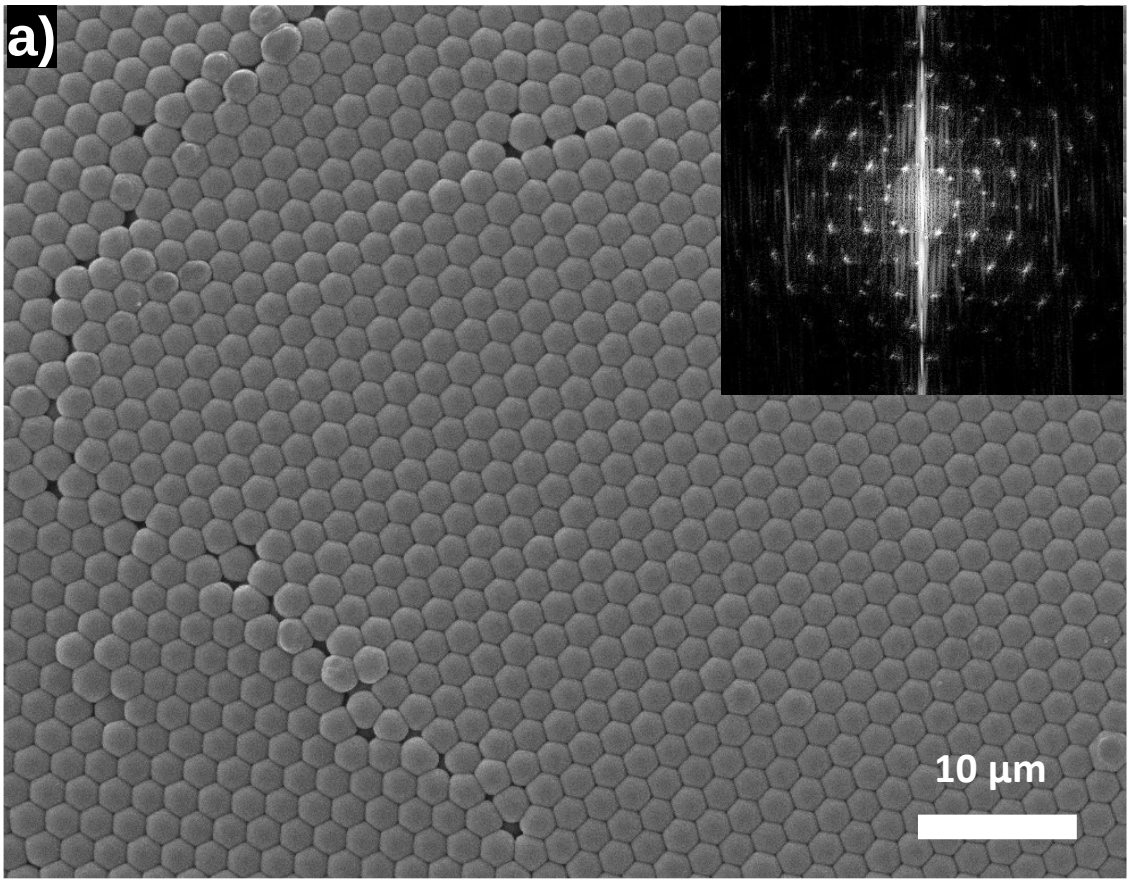


**Figure S13a:** SEM image of the surface of an undoped spherical photonic pigment assembled from PNP260.

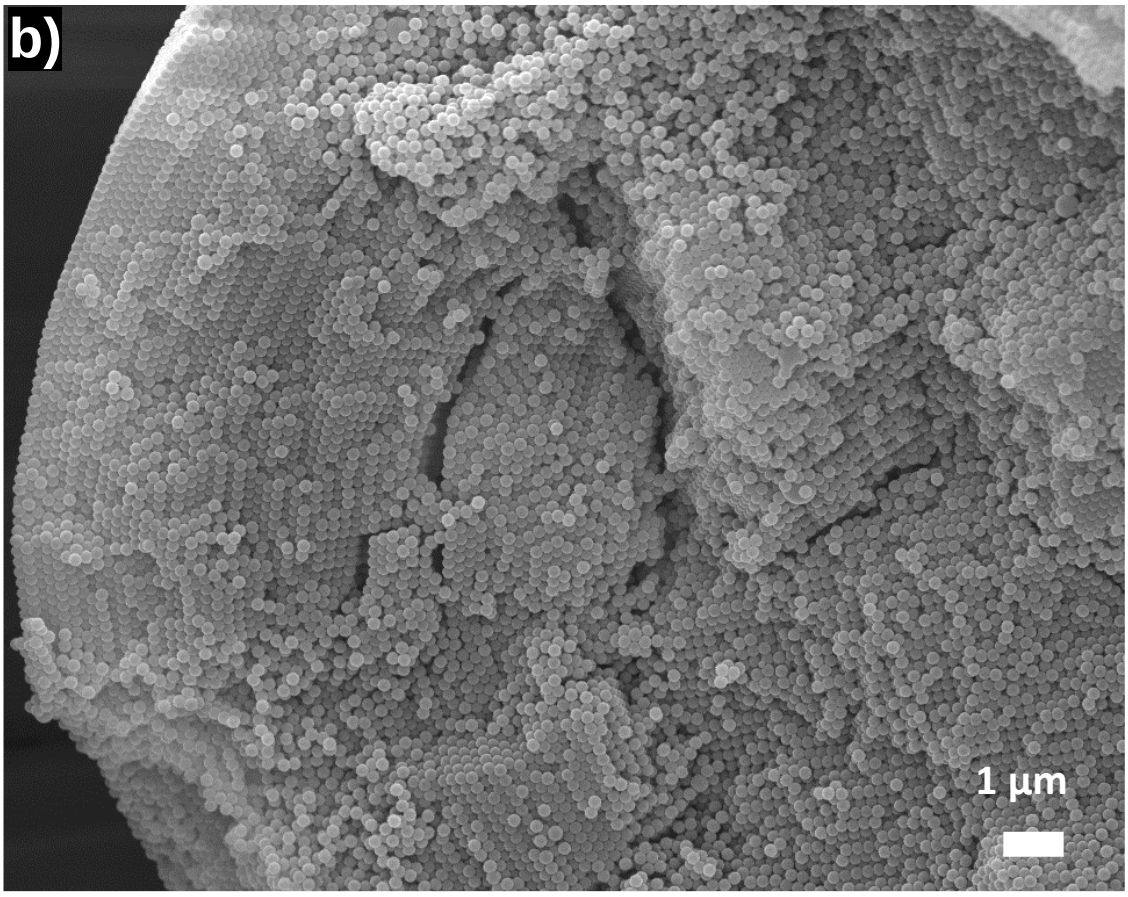


**Figure S13b:** SEM image of the internal structure of an undoped spherical photonic pigment assembled from PNP260.

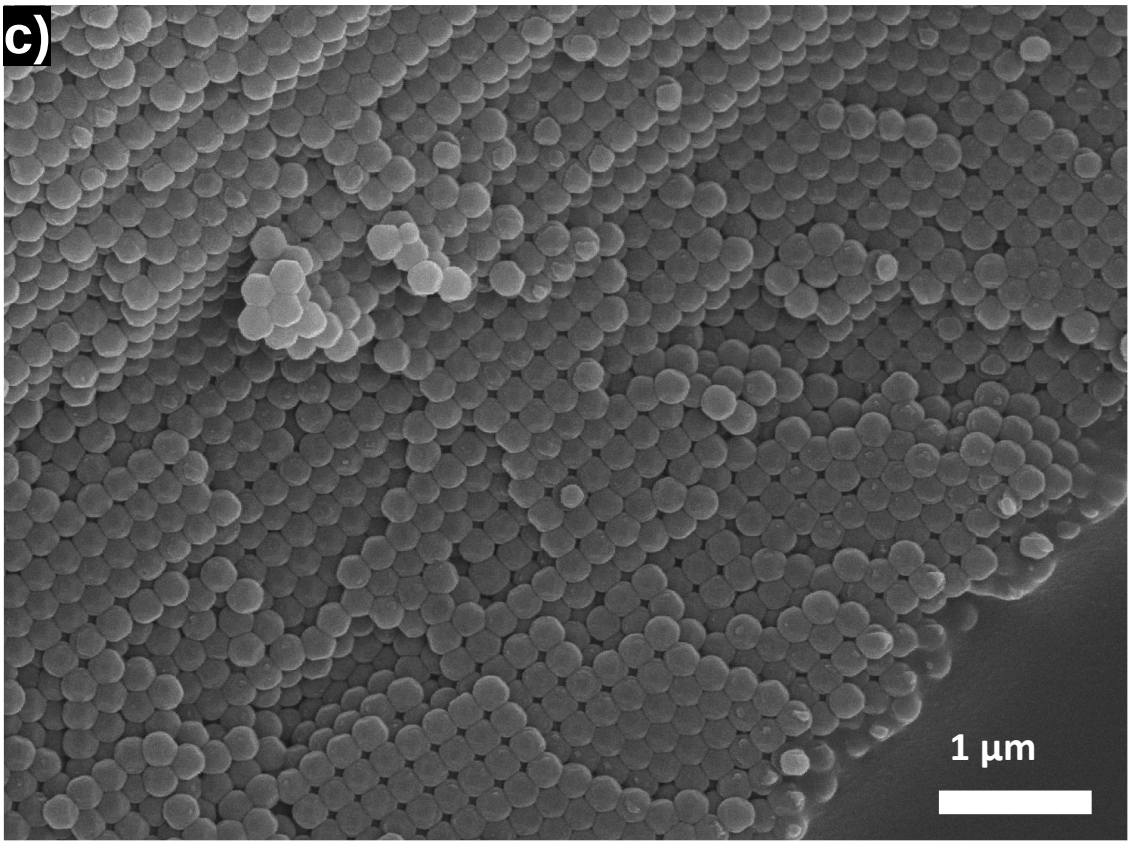


**Figure S13c:** Enlarged SEM image of the internal structure of an undoped spherical photonic pigment assembled from PNP260.

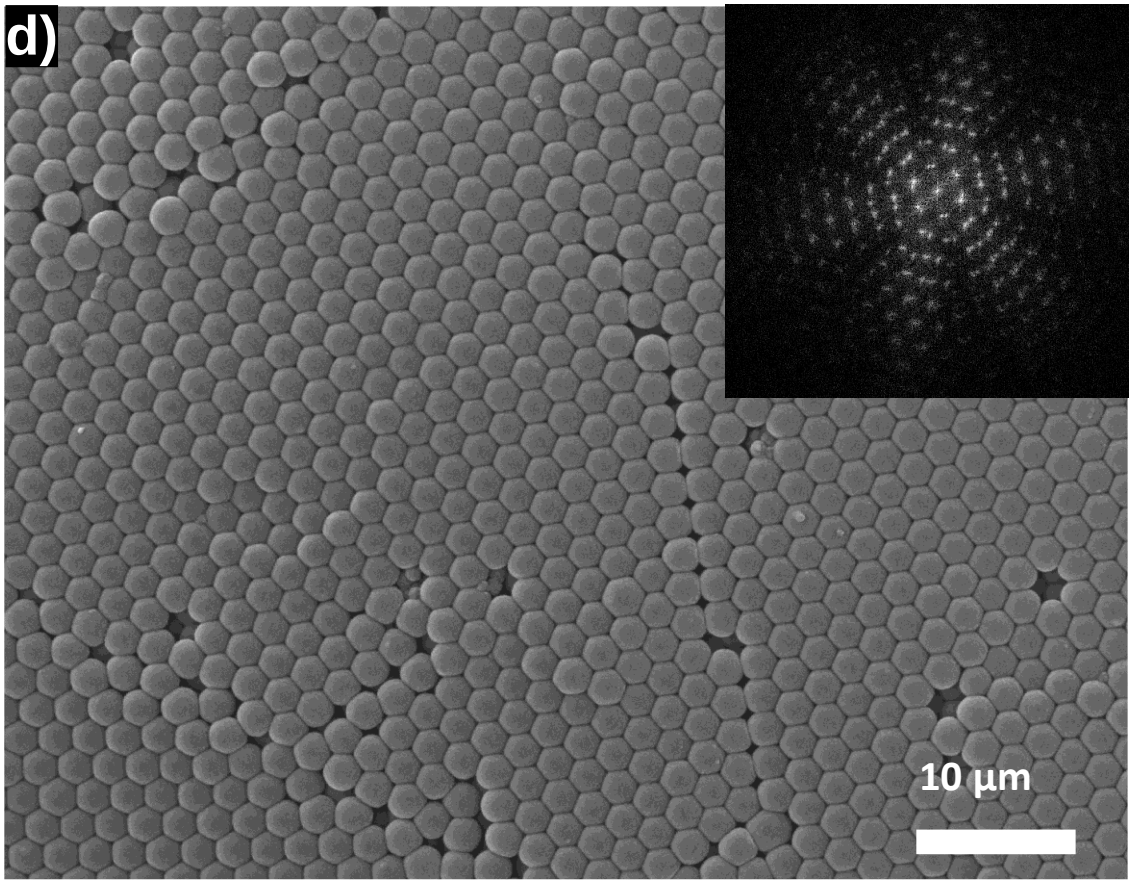


**Figure S13d:** SEM image of the surface of a doped spherical photonic pigment assembled from PNP260.

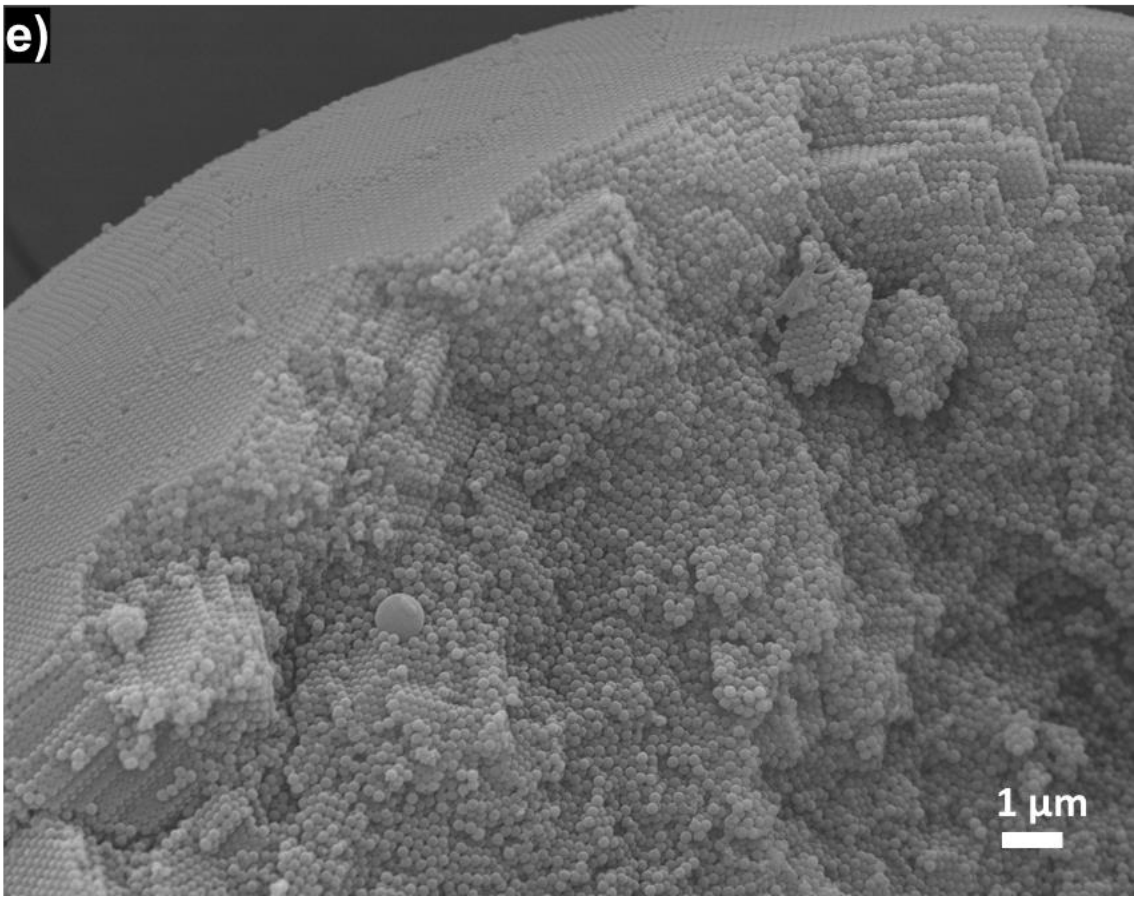


**Figure S13e:** SEM image of the internal structure of a doped spherical photonic pigment assembled from PNP260.

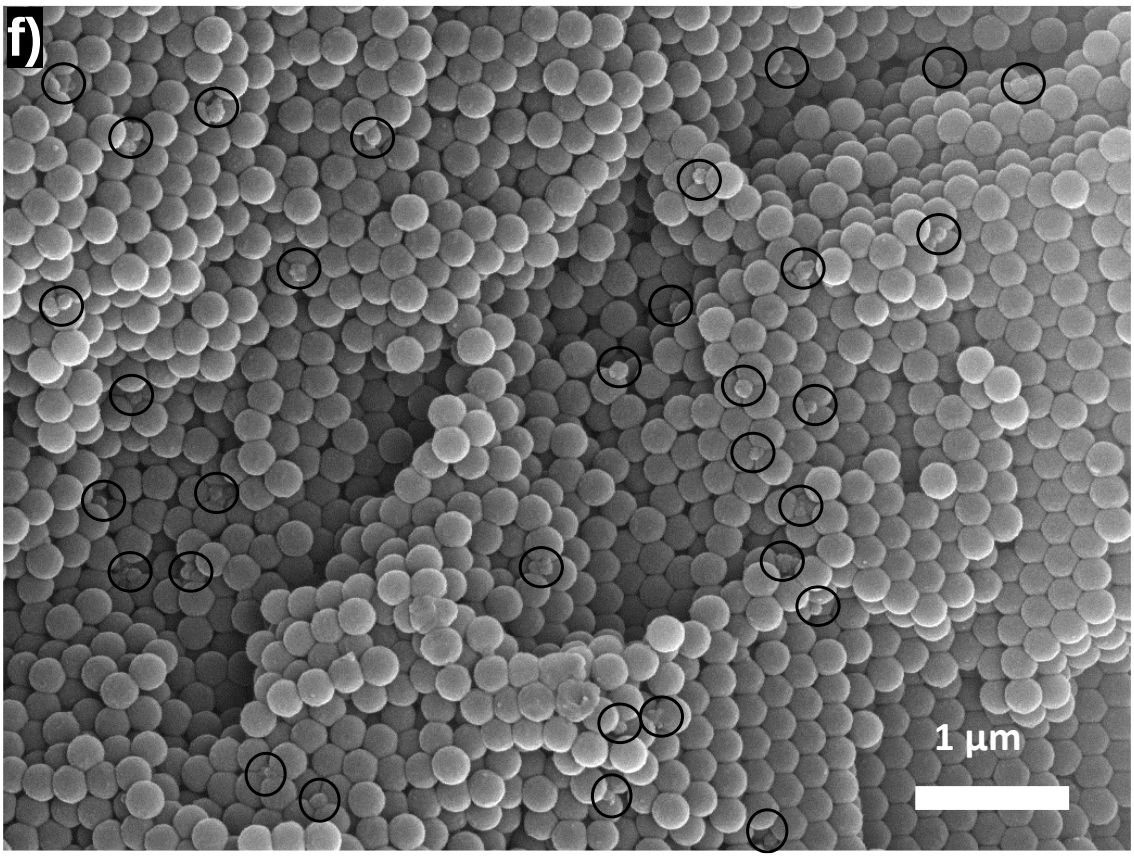


**Figure S13f:** Enlarged SEM image of the internal structure of a doped spherical photonic pigment assembled from PNP260 (black circles highlight the random distribution of PD).

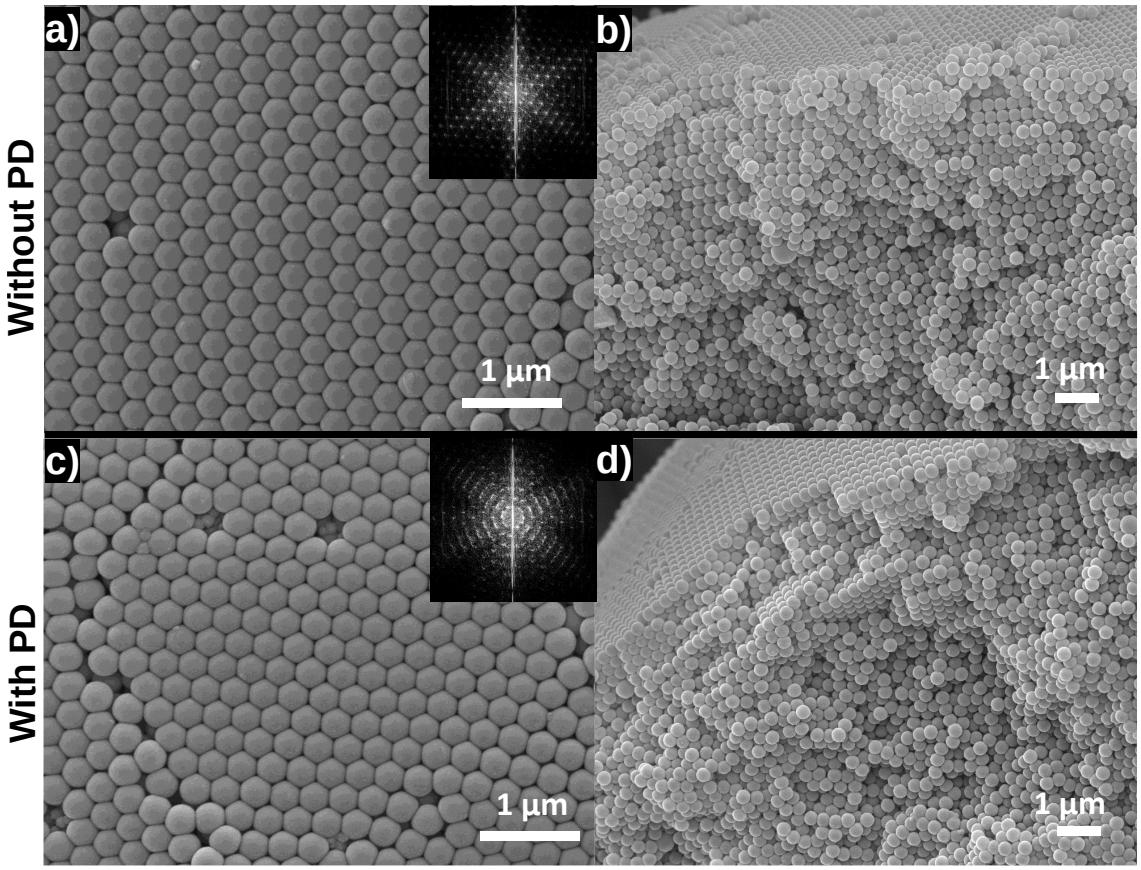


**Figure S14.** SEM images of surface (left panel) and inner structure (right panel) of undoped PhP-PNP318 (**a** and **b**) and doped PhP-PNP318-PD (**c** and **d**) pigments. Inset shows the FFT pattern from the SEM images of the pigments surface. PD is visible in the point defects at pigments surface. Panels **a** to **d** are enlarged in Figures S14a to S14d below.

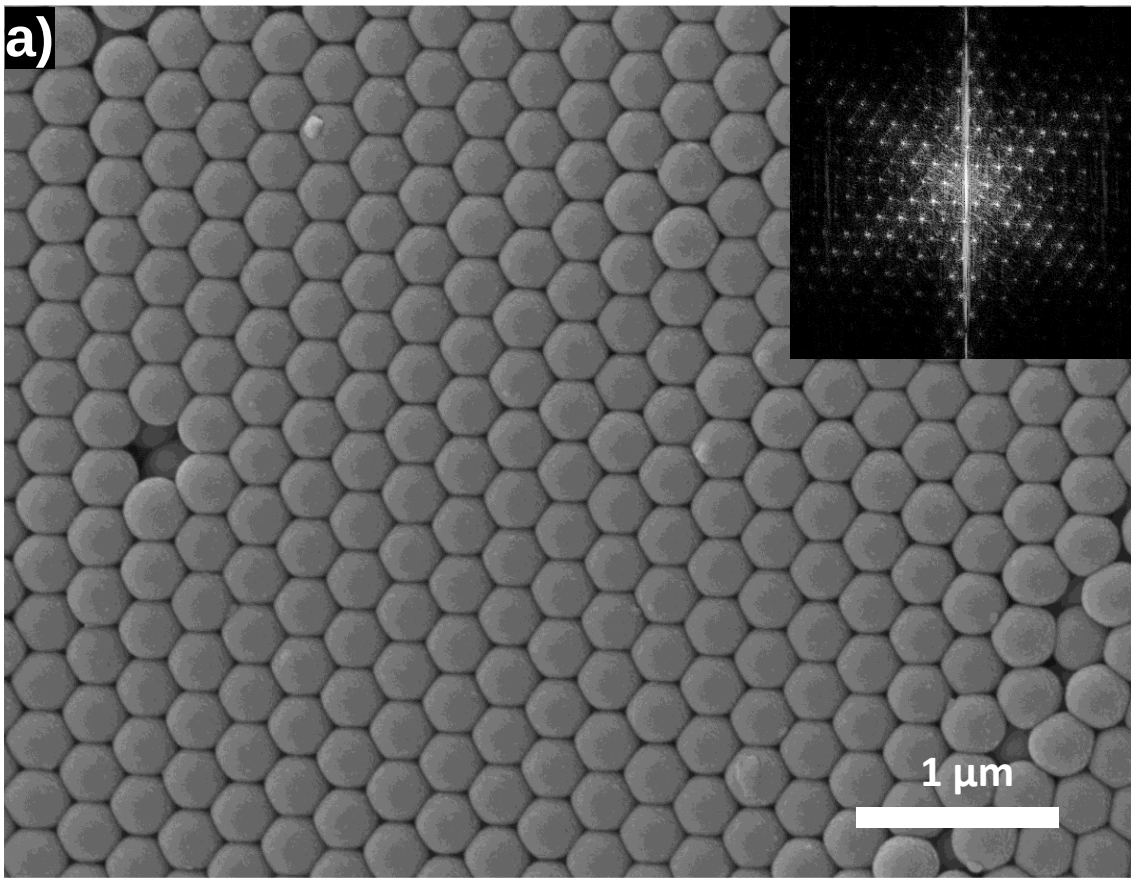


**Figure S14a:** SEM image of the surface of an undoped spherical photonic pigment assembled from PNP318.

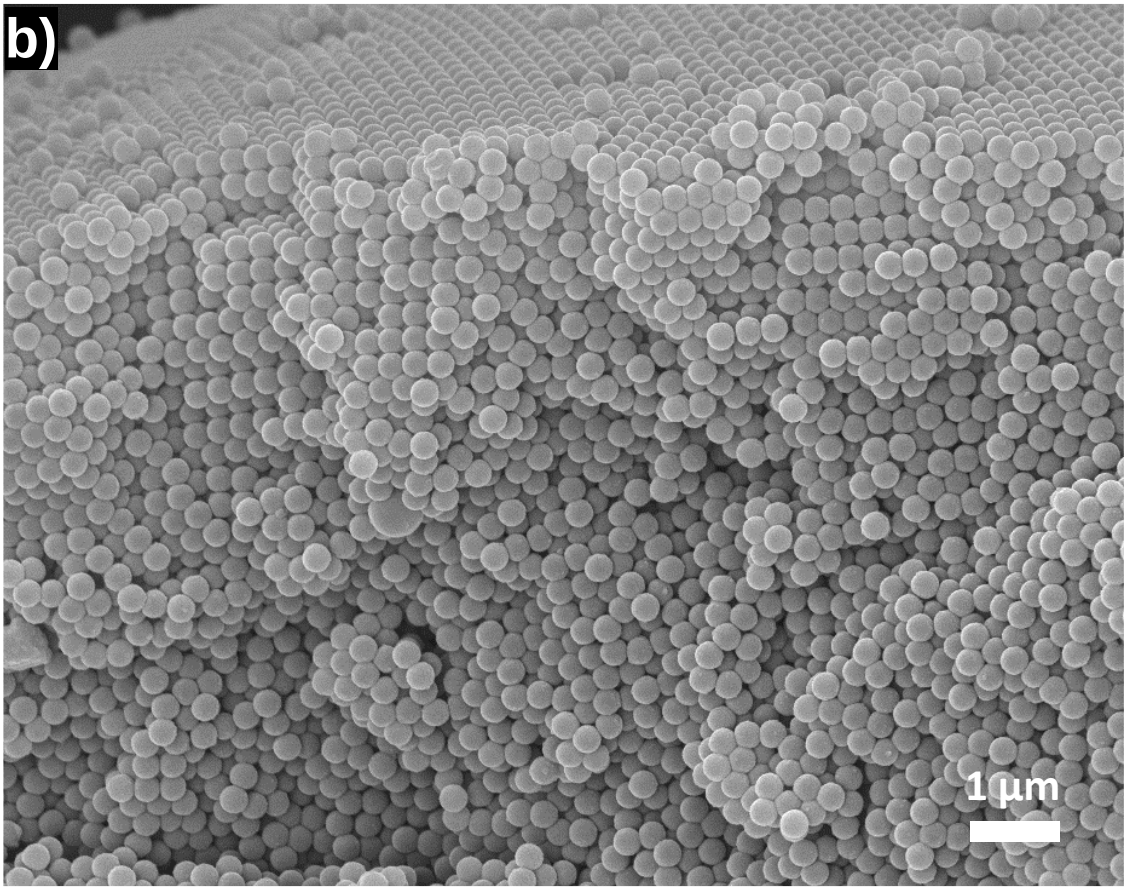


**Figure S14b:** SEM image of the internal structure of an undoped spherical photonic pigment assembled from PNP318.

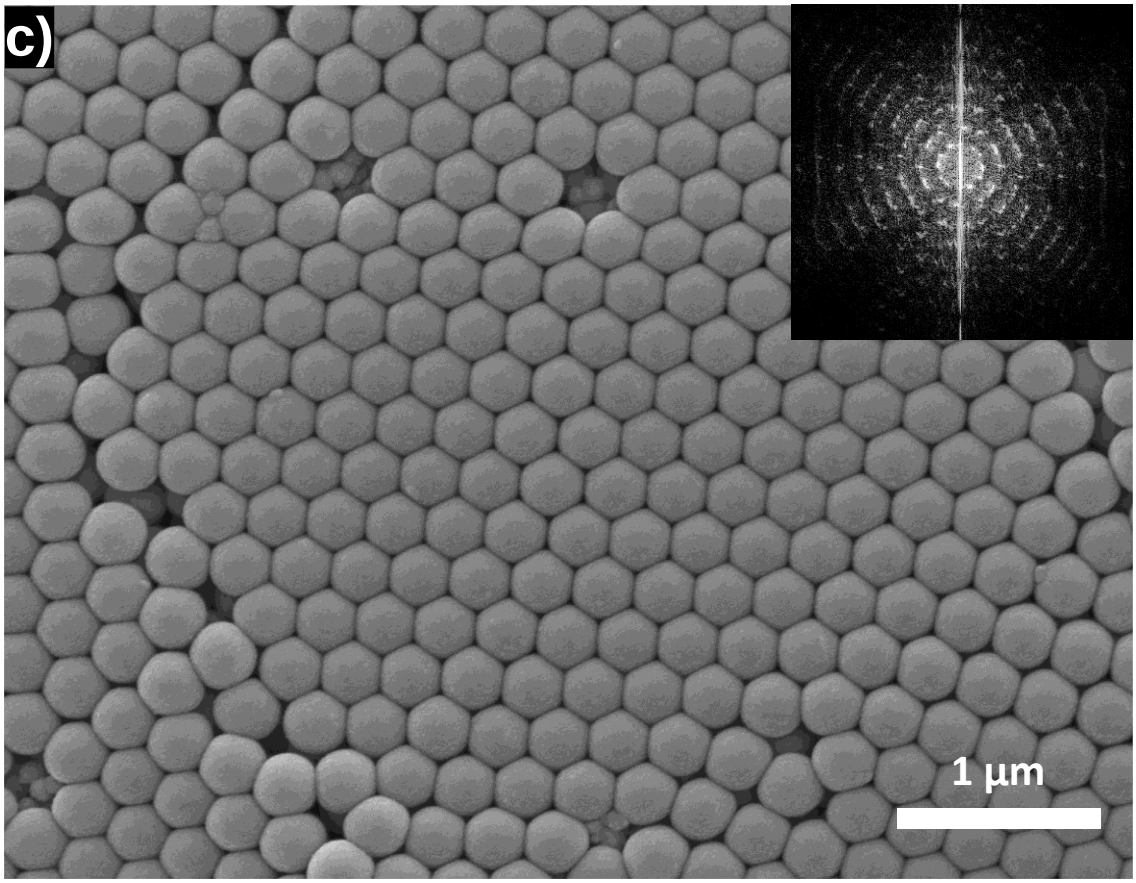


**Figure S14c:** SEM image of the surface of a doped spherical photonic pigment assembled from PNP318.

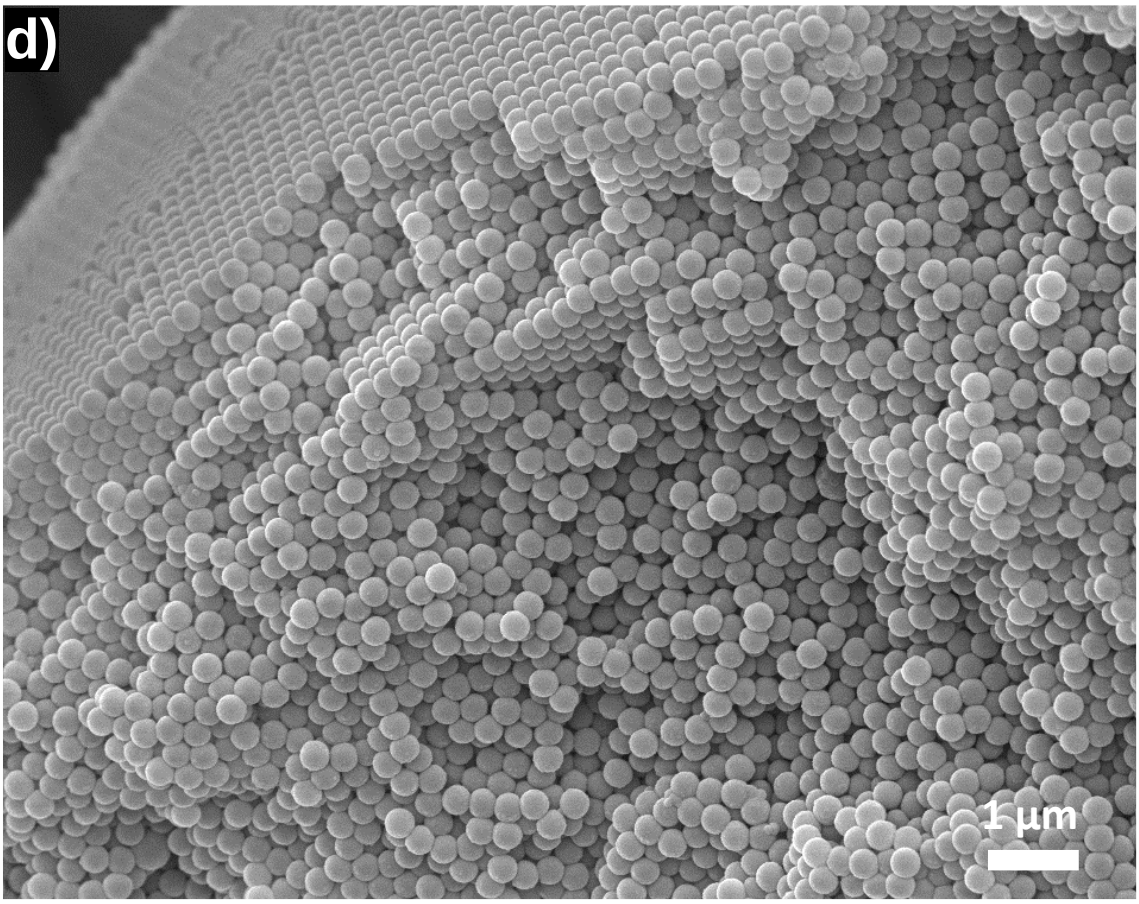


**Figure S14d:** SEM image of the internal structure of a doped spherical photonic pigment assembled from PNP318.

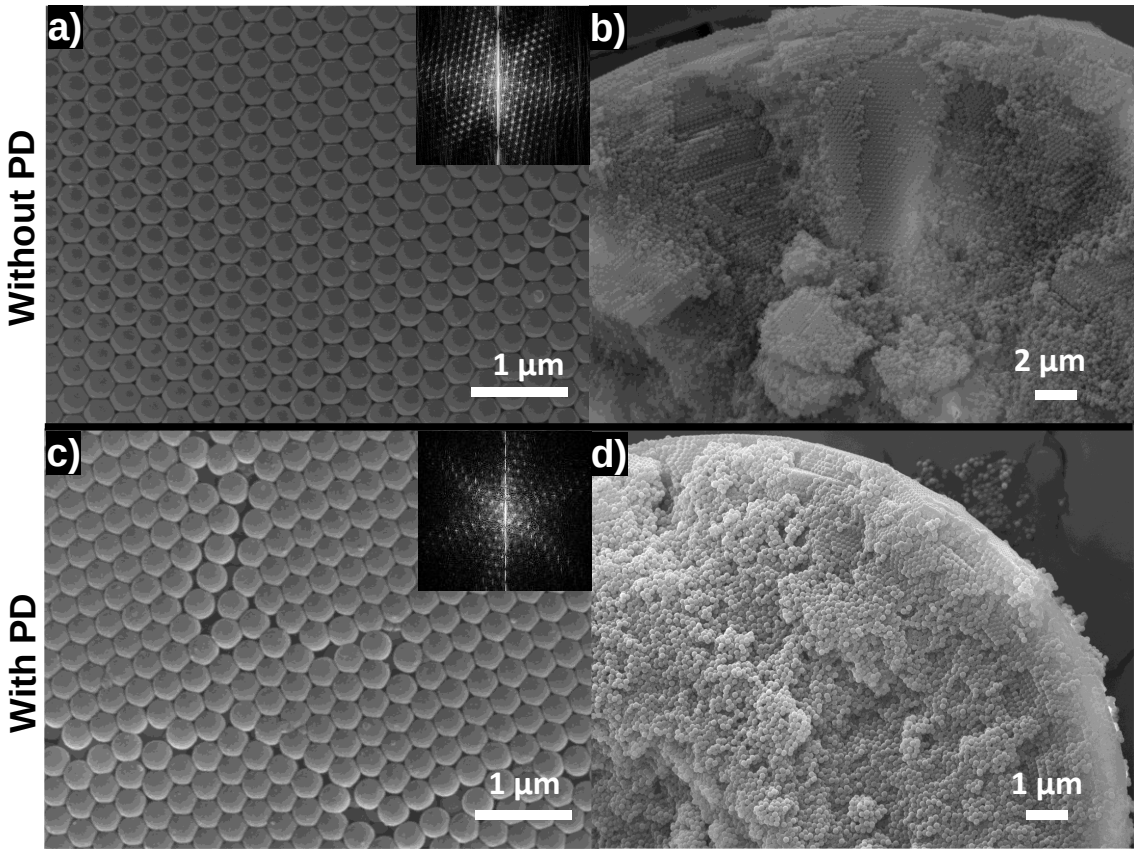


**Figure S15.** SEM images of surface (left panel) and inner structure (right panel) of undoped PhP-PNP331 (**a** and **b**) and doped PhP-PNP331-PD (**c** and **d**) pigments. Inset shows the FFT pattern from the SEM images of the pigments surface. Undoped pigments shows highly ordered PNPs, both at the pigments' surface and in the interior. In contrast, when doped with PD, a more disordered packing of PNPs is visible at the pigment surface, and the number of ordered layers towards the center is lower. Panels **a** to **d** are enlarged in Figures S15a to S15d below.

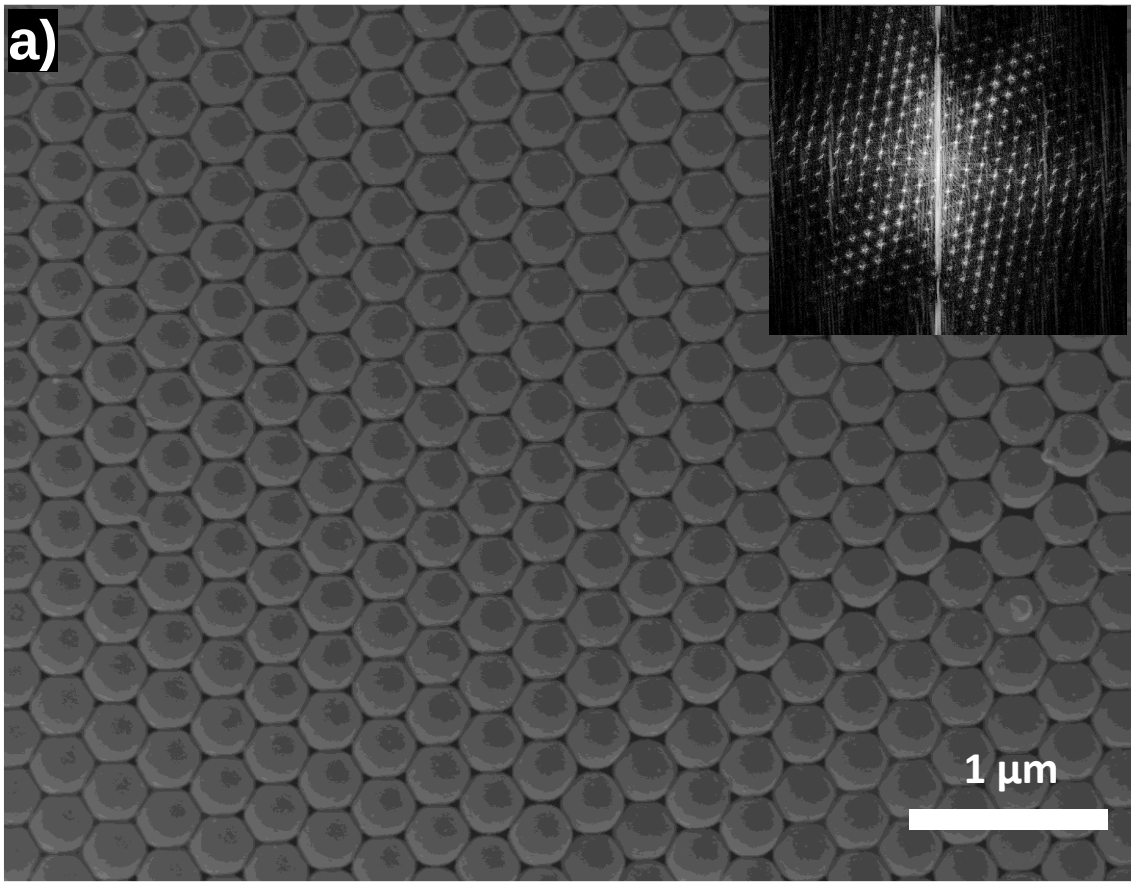


**Figure S15a:** SEM image of the surface of an undoped spherical photonic pigment assembled from PNP331.

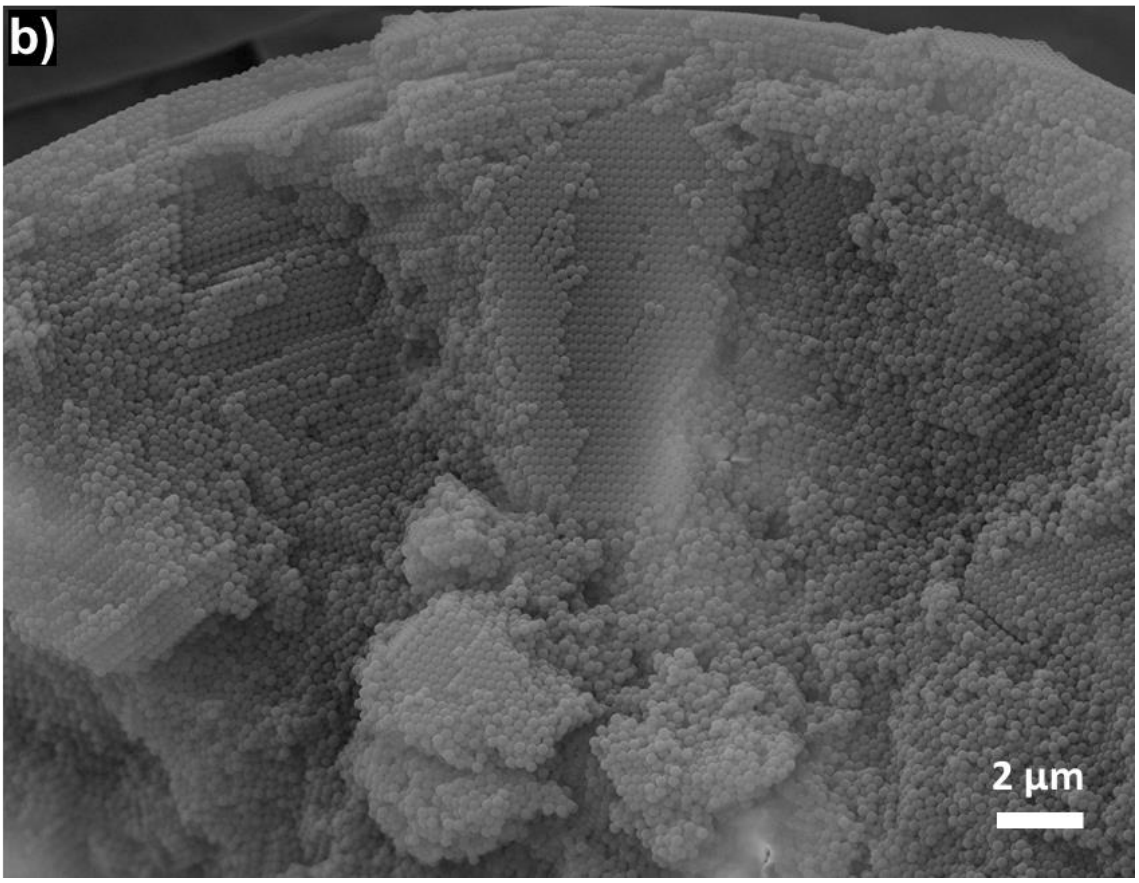


**Figure S15b:** SEM image of the internal structure of an undoped spherical photonic pigment assembled from PNP331.

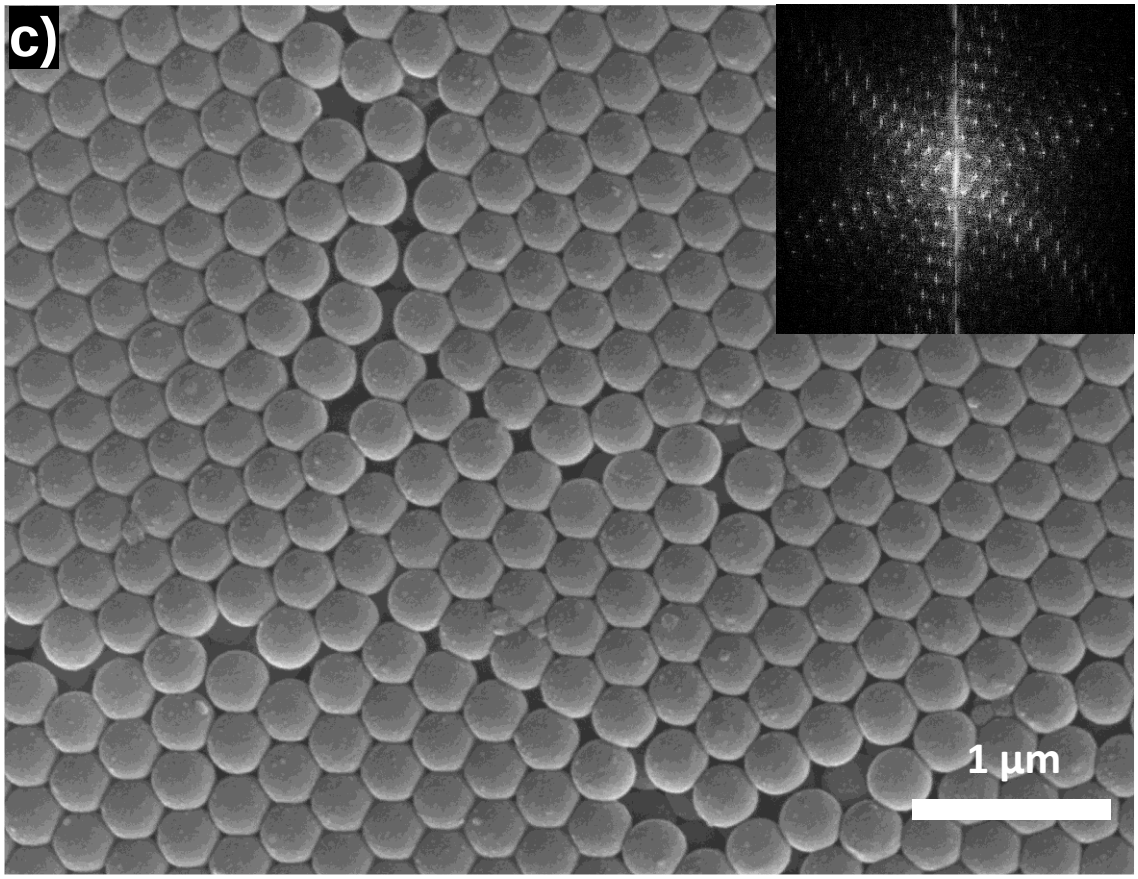


**Figure S15c:** SEM image of the surface of a doped spherical photonic pigment assembled from PNP331.

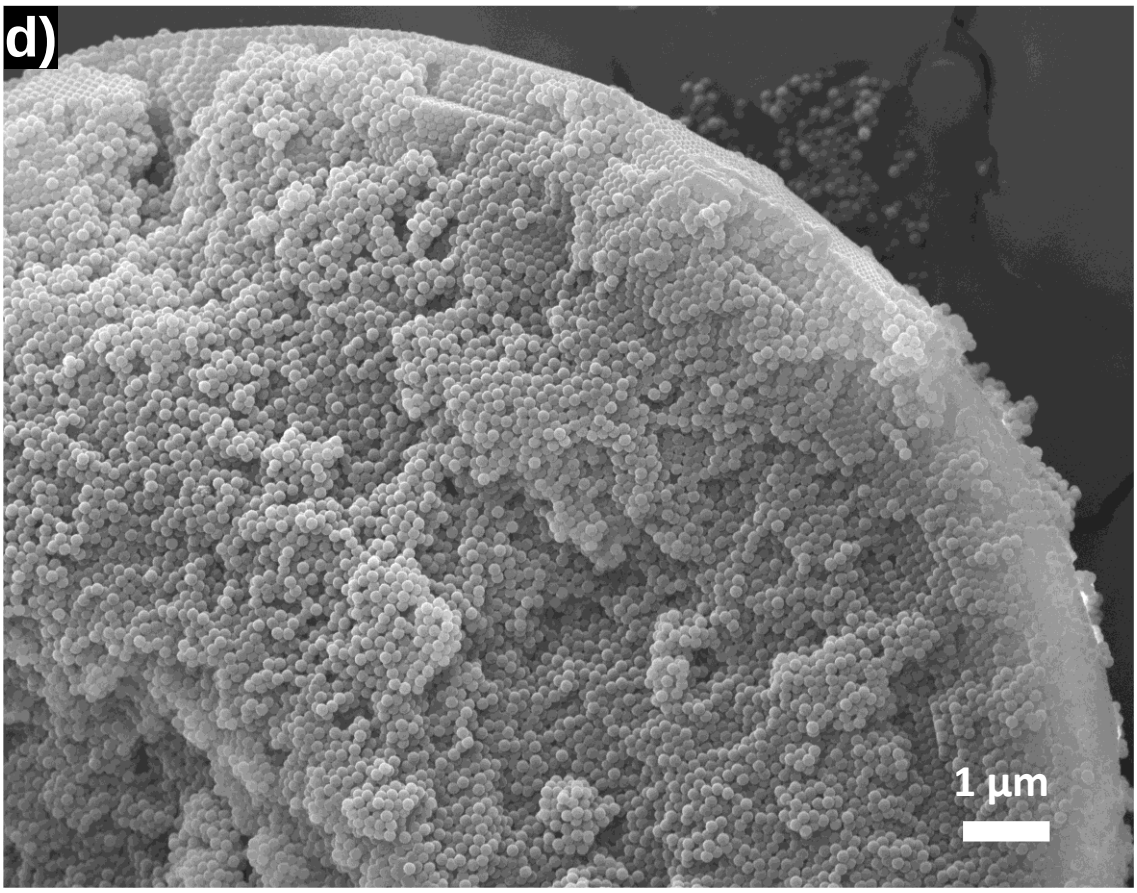


**Figure S15d:** SEM image of the internal structure of a doped spherical photonic pigment assembled from PNP331.

## 5. Reflectance Confocal Microscopy (RCM)

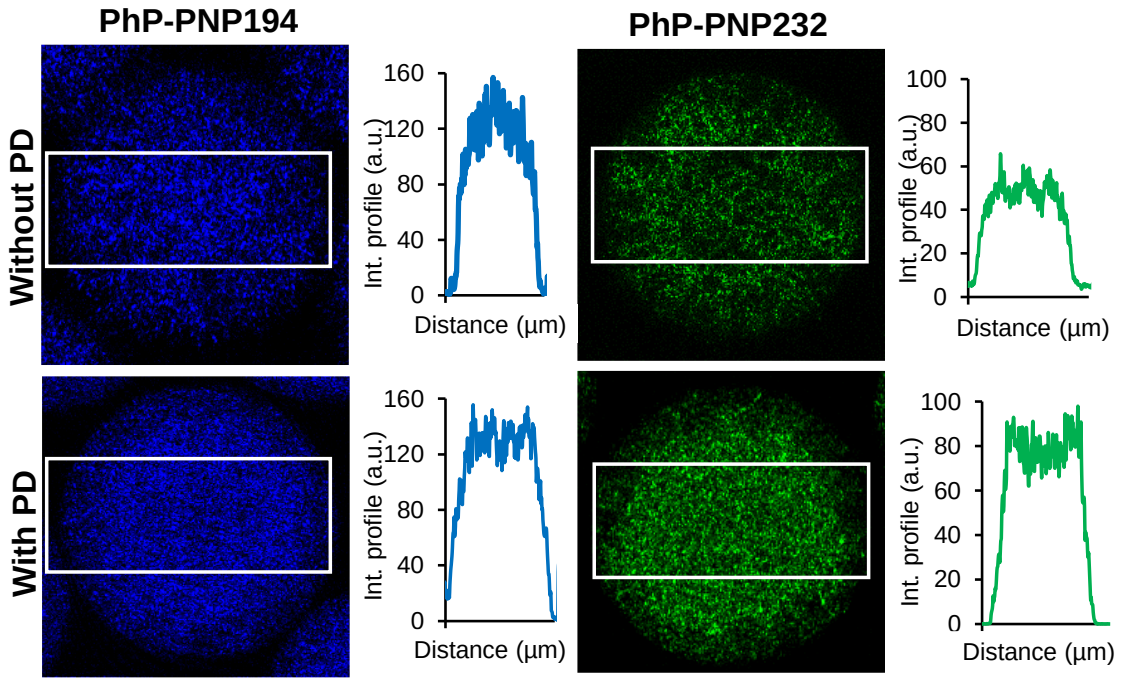


**Figure S16.** RCM images of the equatorial plane of undoped (upper panel) and PD-doped (lower panel) blue and green photonic pigments, imaged under illumination with a 633 nm laser. Since the laser color is outside the structures' bandgap, the images highlight the disordered regions within the structure. The white rectangle denotes the area used to trace the intensity profile of the reflected light. Under this illumination, crystalline planes appear darker, and the regions with more disordered PNP arrangements appear brightly colored. Disorder is especially evident for PD-doped pigments.

## 6. FIB-SEM

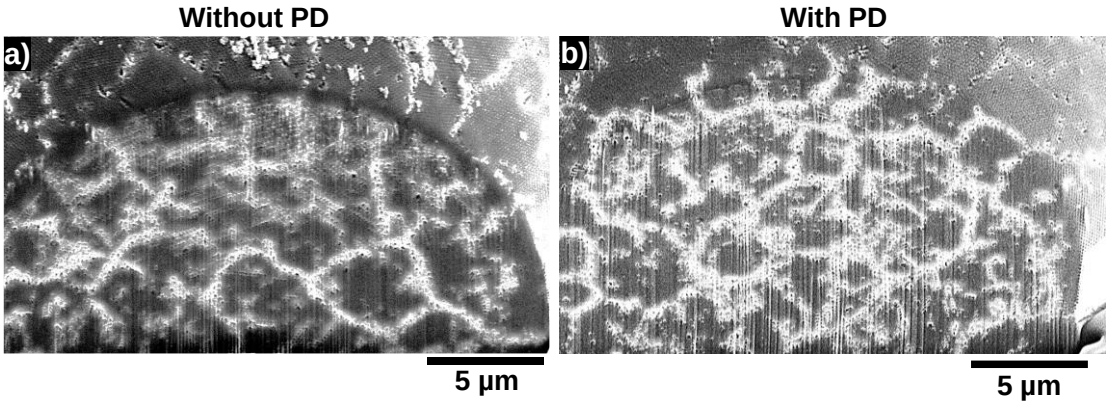


**Figure S17.** FIB-SEM images showing a 5 µm depth cross-section of undoped (**a**) and doped (**b**) pigments composed of PNP232. Defects are visible in both structures, but a higher disorder degree is visible in structures doped with 3 wt% of PD nanoparticles, originating smaller crystalline domains separated by larger disordered boundary regions.